The Forward Speed Diffraction Problem in Following Seas

by

Gregory E. Osborne

B.A., Chemistry
Vanderbilt University (1986)
M.S., Engineering
University of New Orleans (1990)

Submitted to the Department of Ocean Engineering
in partial fulfillment of the requirements for the degree of

Ocean Engineer

at the

MASSACHUSETTS INSTITUTE OF TECHNOLOGY

June 1994

Author .....
.....
Department of Ocean Engineering
April 29, 1994

Certified by.....
.....
J. N. Newman
Professor of Naval Architecture
Thesis Supervisor

Accepted by .....
.....
A. Douglas Carmichael
Professor of Power Engineering
Chairman, Departmental Committee on Graduate Students

The Forward Speed Diffraction Problem in Following Seas

by

Gregory E. Osborne

Submitted to the Department of Ocean Engineering
on April 29, 1994, in partial fulfillment of the
requirements for the degree of
Ocean Engineer

Abstract

When a ship moves through an incident wave field at steady forward speed, it is exposed to forces due to both the oncoming waves and the scattered waves created by the body. The problem of determining the forces attributable to these waves is known as the diffraction problem. Herein, this problem is studied in general along with its particular extension to the special case of a ship travelling at steady forward speed encountering following seas.

The theoretical model for the solution of this problem is based in the time domain and uses linear potential flow theory to determine the forces in terms of impulse-response functions. The case of following seas requires special consideration because the incident wave field is defined with respect to a coordinate system fixed with the ship. Such an incident wave field causes there to be an ambiguity when we try to resolve the wave input. Hence, it is necessary to modify the theory to accommodate this ambiguity.

Numerical results are calculated using the three-dimensional panel code T-MIT. This code is a suite of programs developed at the Computational Hydrodynamics Facility which solves the canonical problems for the velocity potentials and uses them to determine the hydrodynamic quantities in terms of impulse-response functions. Results are presented for a Wigley hull at zero speed and at forward speed in both head seas and following seas.

Thesis Supervisor: J. N. Newman
Title: Professor of Naval Architecture

'The time has come,' the Walrus said,
'To talk of many things:
Of shoes – and ships – and sealing wax –
Of cabbages – and kings –
And why the sea is boiling hot –
And whether pigs have wings.'

– Lewis Carroll

All four winds together
Can't bring the world to me
Shadows hide the play of light
So much I want to see
Chase the light around the world
I want to look at life – In the available light

– Neil Peart

Acknowledgments

I would like to thank my family and friends for all of their support during my time at MIT. I would especially like to thank my mother and father for their unwavering support and encouragement throughout my formative college years.

I also wish to express my sincere appreciation for the guidance of Dr. J. N. Newman in the research and preparation of this thesis. Likewise, I wish to thank Dr. Tom Korsmeyer for the helpful discussions.

The research presented in this thesis was sponsored by the Office of Naval Research, contract number N00014-90-J-1160.

Contents

1 Introduction **15**

2 Mathematical Formulation of the Problem **19**

2.1 Exact Statement of Initial Value Problem 19

2.2 Linearization of the Forward Speed Problem 22

2.3 Scattered Potential Formulation 24

2.4 Diffraction Potential Formulation 28

2.5 The Impulse-Response Function 30

2.6 The Forward Speed Haskind Relations in the Time Domain 31

2.7 Special Case: Following Seas 38

3 Development of the Numerical Scheme **43**

3.1 Panel Methods 43

3.2 Discretization of the Integral Equation 45

3.3 Determination of the Incident Potential 47

3.4 Calculation of the Wave Elevation 58

3.5 Simulation 62

4 Numerical Results **65**

4.1 Zero Speed Results 67

4.2 Forward Speed Results: Head Seas 70

4.3 Forward Speed Results: Following Seas 77

5 Conclusions **93**

List of Figures

4-1 Definition for the incident wave angle heading. 66

4-2 Impulsive Incident Head Wave for the Case of $F_n = 0.0$ and $\beta = \pi$. . 68

4-3 Heave exciting force impulse-response function for a Wigley hull travelling at $F_n = 0.0$ in head seas. 69

4-4 Pitch exciting moment impulse-response function for a Wigley hull travelling at $F_n = 0.0$ in head seas. 70

4-5 Wigley hull at $F_n = 0.0$, $\beta = \pi$, the heave exciting force amplitude. . 71

4-6 Wigley hull at $F_n = 0.0$, $\beta = \pi$, the pitch exciting moment amplitude. 71

4-7 Wigley hull at $F_n = 0.3$, $\beta = \pi$, the heave exciting force impulse-response function. 72

4-8 Wigley hull at $F_n = 0.3$, $\beta = \pi$, the pitch exciting moment impulse-response function. 72

4-9 Comparison of heave exciting force impulse-response functions for a Wigley hull travelling at different forward speeds in head seas. 74

4-10 Comparison of pitch exciting moment impulse-response functions for a Wigley hull travelling at different forward speeds in head seas. 74

4-11 Wigley hull at $F_n = 0.3$, $\beta = \pi$, the heave exciting force amplitude. . 75

4-12 Wigley hull at $F_n = 0.3$, $\beta = \pi$, the pitch exciting moment amplitude. 76

4-13 Wigley hull at $F_n = 0.3$, $\beta = \pi$, the heave exciting force phase angle. 76

4-14 Wigley hull at $F_n = 0.3$, $\beta = \pi$, the pitch exciting moment phase angle. 77

4-15 Example time histories from a simulation of a Wigley hull at $F_n = 0.3$, $\beta = \pi$. From the top: incident wave elevation in the ship-fixed frame, heave response, pitch response. 78

4-16 Wigley hull at $F_n = 0.3$, $\beta = \pi$, the heave response-amplitude operator. 78

4-17 Wigley hull at $F_n = 0.3$, $\beta = \pi$, the pitch response-amplitude operator. 79

4-18 Convergence properties of the heave exciting force impulse-response function for a Wigley hull travelling at $F_n = 0.3$ in following seas where $0 \leq \omega_1 \leq \frac{g}{2U\cos\beta}$. 80

4-19 Convergence properties of the heave exciting force impulse-response function for a Wigley hull travelling at $F_n = 0.3$ in following seas where $\frac{g}{2U\cos\beta} \leq \omega_2 \leq \frac{g}{U\cos\beta}$. 80

4-20 Convergence properties of the heave exciting force impulse-response function for a Wigley hull travelling at $F_n = 0.3$ in following seas where $\frac{g}{U\cos\beta} \leq \omega_3 \leq \infty$. 81

4-21 Convergence properties of the pitch exciting moment impulse-response function for a Wigley hull travelling at $F_n = 0.3$ in following seas where $0 \leq \omega_1 \leq \frac{g}{2U\cos\beta}$. 81

4-22 Convergence properties of the pitch exciting moment impulse-response function for a Wigley hull travelling at $F_n = 0.3$ in following seas where $\frac{g}{2U\cos\beta} \leq \omega_2 \leq \frac{g}{U\cos\beta}$. 82

4-23 Convergence properties of the pitch exciting moment impulse-response function for a Wigley hull travelling at $F_n = 0.3$ in following seas where $\frac{g}{U\cos\beta} \leq \omega_3 \leq \infty$. 82

4-24 Comparison of heave exciting force impulse-response functions for a Wigley hull travelling at different forward speeds in following seas where $0 \leq \omega_1 \leq \frac{g}{2U\cos\beta}$. 84

4-25 Comparison of pitch exciting moment impulse-response functions for a Wigley hull travelling at different forward speeds in following seas where $0 \leq \omega_1 \leq \frac{g}{2U\cos\beta}$. 84

4-26 Comparison of heave exciting force impulse-response functions for a Wigley hull travelling at different forward speeds in following seas where $\frac{g}{2U\cos\beta} \leq \omega_2 \leq \frac{g}{U\cos\beta}$. 85

4-27 Comparison of pitch exciting moment impulse-response functions for a Wigley hull travelling at different forward speeds in following seas where $\frac{g}{2U\cos\beta} \leq \omega_2 \leq \frac{g}{U\cos\beta}$. 85
4-28 Extended time histories of the heave exciting force impulse-response functions for a Wigley hull travelling at $F_n = 0.3$ in following seas. . . 86
4-29 Extended time histories of the pitch exciting moment impulse-response functions for a Wigley hull travelling at $F_n = 0.3$ in following seas. . . 87
4-30 Heave exciting force amplitudes for a Wigley hull travelling at $F_n = 0.3$ in following seas. 89
4-31 Pitch exciting moment amplitudes for a Wigley hull travelling at $F_n = 0.3$ in following seas. 89
4-32 Heave exciting force amplitude with respect to absolute frequency for a Wigley hull travelling at $F_n = 0.3$ in following seas. 90
4-33 Heave exciting force phase angle with respect to absolute frequency for a Wigley hull travelling at $F_n = 0.3$ in following seas. 90
4-34 Pitch exciting moment amplitude with respect to absolute frequency for a Wigley hull travelling at $F_n = 0.3$ in following seas. 91
4-35 Pitch exciting moment phase angle with respect to absolute frequency for a Wigley hull travelling at $F_n = 0.3$ in following seas. 91

Chapter 1

Introduction

The problem with which this thesis is concerned is the determination of forces and motions of a vessel due to operation at steady forward speed in an infinite seaway. In particular, we are interested in the ship's reactions in the presence of an ambient wave field where body motions may be attributed to both the oncoming waves and the scattering of these waves. This class of problem is known as the diffraction problem. Furthermore, we are interested in developing a three-dimensional method for solving this problem in the time domain.

Explorations for solutions to the zero speed diffraction problem have been thorough and are well documented. The first innovations in the realm of wave force approximations occurred in the middle and late nineteenth century with the theories of Froude [6] in 1861 and Krilov [13] in 1896. Their method consists of integrating the pressure due to a sinusoidal wave in the absence of a diffracting body. The pressure is determined using a linearized Bernoulli equation, and the resulting quantity has come to be known as the Froude-Krilov force. This force is an important component in the overall diffraction problem as will be seen later in this text.

A further innovation in this area was presented by Haskind [8] in 1957. Here, Haskind postulated that the overall ship motions problem could be decomposed into separate parts. He went on to show the exciting forces (which are due to the incident and scattered waves) may be found by the solution of a different problem, i.e., the radiation problem. In this case, we find the forces which are caused by radiated

waves occurring when the ship makes small perturbations about its mean position. Hence the Haskind relations, as they are known, provide a means of calculating the forces at zero speed by solving only the radiation problem. Such an approach is quite computationally efficient and very useful when only forces for a nontranslating object are desired.

Haskind's work was done in the frequency domain, and so in 1967 Wehausen [21] presented analogous results in the time domain. Likewise, the fact that the Haskind relations only apply to the case of zero forward speed begged for improvement. Thus, in 1965 Newman [16] extended Haskind's frequency-domain relations to the case of a body moving at steady forward speed. The forward speed relations are restricted in their usefulness, however, since the free-surface boundary condition makes it necessary to employ reverse-flow radiation potentials which are not normally calculated. Likewise, it must be assumed that the ship is thin. Analogous time-domain relations are presented for the first time later in this thesis.

There has also been additional noteworthy work in the regime of time-domain solutions to the ship motions problem. The topic was originally extensively discussed by Cummins [3] and reinterpreted by Ogilvie [17]. In 1971, Wehausen [22] presented a time-domain boundary integral method following that originally initiated by Volterra [20]. This method uses an application of Green's theorem to the time derivative of the velocity potential and an appropriate Green's function to obtain a Fredholm integral equation of the second kind. Solution of Wehausen's integral equation provides the velocity potential for a ship with zero forward speed. Most recently, extensions in the theory have been made to include three-dimensional time-domain solutions for a ship translating at steady forward speed. Such innovations may be found in King [11], which includes the diffraction problem, and Bingham et al. [2], which contains some of the results presented in this thesis.

Most of the previous work in the area of time-domain ship motions analysis has concentrated on solution of the radiation problem, and that which discusses the diffraction problem spends little time with the specific case of following seas. This thesis will attempt to clarify the subject by providing an overview of the applicable

theory and showing a variety of numerical results covering the main classifications of ship speeds and wave headings, most notably results for a ship moving with steady forward speed in following seas.

The main body of this thesis is divided into three sections. The first section, contained in Chapter 2, illustrates the theory used in developing a linearized three-dimensional time-domain boundary integral equation method for the solution of the diffraction problem. This theory includes the simplifying assumptions that are necessary in developing the model as well as a derivation of the second kind Fredholm integral equation and a discussion of the incident wave potential and the special considerations needed for solving the following seas case. Also, as mentioned earlier, a derivation of the forward speed Haskind relations in the time domain is presented in this chapter.

The second section, contained in Chapter 3, provides a discussion of the numerical aspects of solving for the diffraction potential. Included in this discussion are a brief overview of three-dimensional panel methods, which are used for the numerical solution of the integral equation, and a presentation of the analytical methods with which various quantities of the incident potential and wave elevation are solved. This chapter also contains a short explanation of how ship motions are numerically calculated through simulation.

The third section, contained in Chapter 4, shows the numerical results obtained by application of the theory and numerics found in Chapter 2 and Chapter 3. These results are presented for the case of zero speed as well as for steady forward speed in both head and following seas.

Finally, Chapter 5 provides a few concluding remarks and discussion of possible future work.

Chapter 2

Mathematical Formulation of the Problem

2.1 Exact Statement of Initial Value Problem

For the problem of determining the motions of a freely floating surface piercing vessel in a seaway, we consider the model of a three-dimensional body in a semi-infinite fluid with a free-surface. In addition, we assume the vessel translates with steady velocity U through an incident wave field and undergoes small oscillations about its mean position. The ship's position may be described with respect to an inertial coordinate system, $\vec{x_o}$, which is fixed in space or with respect to a moving coordinate system, $\vec{x}$, which is fixed at the mean position of the ship. The origin of the inertial coordinate system is defined such that it coincides with the origin of the ship fixed coordinate system at time t=0.

In order to evaluate the physical problem, we make the simplifying assumptions that the fluid is both inviscid and incompressible and that the flow is irrotational. We can therefore describe the fluid velocity field in terms of the gradient of its potential, that is,

$$\vec{V}(\vec{x_o}, t) = \vec{\nabla}\Phi(\vec{x_o}, t). \tag{2.1}$$

Given these assumptions, the principle of mass conservation dictates that the velocity potential is a solution to Laplace's equation

$$\nabla^2\Phi = 0 \qquad \text{in fluid domain.} \tag{2.2}$$

We may then find the pressure field, $p(\vec{x_o}, t)$, in the inertial coordinate system from Bernoulli's equation

$$p - p_a = -\rho(\Phi_t + \frac{1}{2}\vec{\nabla}\Phi \cdot \vec{\nabla}\Phi + gz_o) \tag{2.3}$$

where ρ is the fluid density, g is the gravitational acceleration, and p_a is the atmospheric pressure, which is used as the reference pressure and assumed constant.

We must now define the problem boundary conditions. On the submerged portion of the body surface, the velocity of the fluid in the direction normal to the body must equal the velocity of the body

$$\vec{n} \cdot \vec{\nabla}\Phi = \vec{V_s} \cdot \vec{n} \qquad \text{on } S_b(t) \tag{2.4}$$

where $\vec{V_s}(\vec{x_o}, t)$ is the velocity of a point on the body, $S_b(t)$ is the exact position of the body's submerged surface, and $\vec{n}$ is the body's unit normal vector. The conditions at the free-surface can be defined in terms of a kinematic and a dynamic boundary condition. Because the free-surface is a material surface, we can state the free-surface kinematic boundary condition in terms of the substantial derivative

$$\frac{D}{Dt}(z_o - \zeta) = (\frac{\partial}{\partial t} + \vec{\nabla}\Phi \cdot \vec{\nabla})(z_o - \zeta) = 0 \qquad \text{on } z_o = \zeta, \tag{2.5}$$

where $\zeta(x_o, y_o, t)$ is the unknown free-surface elevation. Furthermore, we can obtain

the dynamic free-surface boundary condition by taking the pressure on the free-surface as equal to atmospheric pressure:

$$\Phi_t + \frac{1}{2}\vec{\nabla}\Phi \cdot \vec{\nabla}\Phi + gz_o = 0 \qquad \text{on } z_o = \zeta. \tag{2.6}$$

Neglecting surface tension, we can obtain the unknown wave elevation from (2.6)

$$\zeta(x_o, y_o, t) = -\frac{1}{g}(\Phi_t + \frac{1}{2}\vec{\nabla}\Phi \cdot \vec{\nabla}\Phi)_{z_o=\zeta} \tag{2.7}$$

and using the substantial derivative, we may eleminate ζ and get the combined free-surface boundary condition

$$\Phi_{tt} + 2\vec{\nabla}\Phi \cdot \vec{\nabla}\Phi_t + \frac{1}{2}\vec{\nabla}\Phi \cdot \vec{\nabla}(\vec{\nabla}\Phi \cdot \vec{\nabla}\Phi) + g\Phi_{z_o} = 0 \qquad \text{on } z_o = \zeta. \tag{2.8}$$

Because the fluid is semi-infinite, we must also satisfy a condition as $|\vec{x}| \to \infty$. Simply stated, for finite time periods, the velocity of the body disturbance decays to undisturbed flow as it moves toward spatial infinity

$$\vec{\nabla}\Phi \to 0 \qquad \text{as } x, y \to \infty \tag{2.9}$$

and

$$\vec{\nabla}\Phi \to 0 \qquad \text{as } z \to -\infty. \tag{2.10}$$

Finally, because the free-surface boundary condition is second order in time, it is necessary to specify two initial conditions

$$\Phi = 0 \quad \text{on} \quad z_o = 0, \quad t \to -\infty$$
$$\Phi_t = 0 \quad \text{on} \quad z_o = 0, \quad t \to -\infty. \tag{2.11}$$

2.2 Linearization of the Forward Speed Problem

The problem as we have outlined it above is nonlinear. This is not only due to the nonlinearities found in the free-surface boundary condition but also its application over an unknown wave elevation (2.7). We would therefore like to simplify this problem further by linearizing the boundary conditions and Bernoulli's equation. We use the form shown in [2] and begin by decomposing the velocity potential in the form

$$\Phi(\vec{x},t) = \bar{\Phi}(\vec{x}) + \bar{\phi}(\vec{x}) + \sum_{k=1}^{6} \phi_k(\vec{x},t) + \phi^I(\vec{x},t) + \phi^S(\vec{x},t) \tag{2.12}$$

where we are now using the ship-fixed coordinate system. We assume that the ship is translating with steady speed U in the x_o direction and that the flow is no longer affected by transients due to ship acceleration. The potential as defined in (2.12) can be expressed in terms of its steady and unsteady components. The steady components of the potential, $\bar{\Phi}(\vec{x})$ and $\bar{\phi}(\vec{x})$, correspond to the disturbance created by the steady forward translation of the ship. The remaining potential components are due to unsteady motions of the fluid. The radiation potential, $\phi_k(\vec{x},t)$, results from unsteady disturbances created when the translating ship is forced in a prescribed way in a particular rigid body mode of motion. These modes coincide with the ship's six degrees of freedom. The incident potential, $\phi^I(\vec{x},t)$, corresponds to the incident wave field through which the ship passes. Lastly, the scattered potential, $\phi^S(\vec{x},t)$, is due to the scattering caused when the ship encounters the incident wave field. We will define the diffraction potential as the sum

$$\phi^D(\vec{x},t) = \phi^I(\vec{x},t) + \phi^S(\vec{x},t) \tag{2.13}$$

Returning to the decomposition of the potential (2.12), we assume that velocities associated with the steady potential $\bar{\Phi}(\vec{x})$ are $\mathcal{O}(1)$ and all other velocities are small perturbations about the flow described by $\bar{\Phi}(\vec{x})$. We will call the $\mathcal{O}(1)$ flow the basis flow. We require that the basis flow approaches free stream flow as we move far from the ship but we make no other restriction on choice of $\bar{\Phi}(\vec{x})$. Given this fact, we choose to use the most simple basis flow, that is, the free stream itself

$$\bar{\Phi}(\vec{x}) = -Ux. \tag{2.14}$$

Using this basis flow and substituting (2.12) into the expressions for the boundary conditions and Bernoulli equation yields the Neumann-Kelvin linearization of the initial value problem:

$$p = -\rho(\phi_t - U\phi_x) \tag{2.15}$$

$$(\frac{\partial}{\partial t} - U\frac{\partial}{\partial x})^2\phi + g\frac{\partial \phi}{\partial z} = 0 \qquad \text{on } z = 0 \tag{2.16}$$

$$\begin{aligned} \vec{n}\cdot\vec{\nabla}\bar{\phi} &= Un_1 \\ \vec{n}\cdot\vec{\nabla}\phi^D &= 0 \\ \vec{n}\cdot\vec{\nabla}\phi_k &= n_k\dot{x_k} + m_k x_k \end{aligned} \tag{2.17}$$

where ϕ can be ϕ_k, ϕ^I, or ϕ^S and all body boundary conditions are applied on the mean position of the ship surface, S_b. Likewise, we define n_k as the k^{th} component of the generalized unit normal which for the six rigid body modes of motion are

$$\begin{aligned}(n_1, n_2, n_3) &= \vec{n} \\ (n_4, n_5, n_6) &= \vec{r} \times \vec{n}.\end{aligned} \tag{2.18}$$

The 'm-terms' which we see in the body boundary condition for the radiation problem are a manifestation of coupling between the steady and unsteady potentials and are defined as

$$\begin{aligned}(m_1, m_2, m_3) &= -(\vec{n} \cdot \vec{\nabla})\vec{\nabla}\bar{\Phi}(\vec{x}) \\ (m_4, m_5, m_6) &= -(\vec{n} \cdot \vec{\nabla})(\vec{r} \times \vec{\nabla}\bar{\Phi}(\vec{x}))\end{aligned} \tag{2.19}$$

which, given our choice of basis flow, reduce to

$$m_k = (0, 0, 0, 0, Un_3, -Un_2). \tag{2.20}$$

2.3 Scattered Potential Formulation

For the linearized initial value problem, we define the scattered potential, $\phi^S(\vec{x}, t)$, as the solution to Laplace's equation

$$\nabla^2 \phi^S(\vec{x}, t) = 0 \qquad \text{in } V \tag{2.21}$$

and constrained by the following boundary conditions:

$$\left(\frac{\partial}{\partial t} - U\frac{\partial}{\partial x}\right)^2 \phi^S + g\frac{\partial \phi^S}{\partial z} = 0 \qquad \text{on } S_F \tag{2.22}$$

$$\vec{n}\cdot\vec{\nabla}\phi^S = -\vec{n}\cdot\vec{\nabla}\phi^I \qquad \text{on } S_B \tag{2.23}$$

$$\vec{\nabla}\phi^S \to 0 \qquad \text{on } S_\infty \text{ for } t \text{ finite} \tag{2.24}$$

We should also note that both ϕ^S and ϕ^S_t are uniformly bounded on S_∞ for finite t. Because the free surface boundary condition is second order in time, it is necessary that we specify two initial conditions. Therefore, we also require:

$$\phi^S(\vec{x},t) \to 0 \quad t \to -\infty \tag{2.25}$$

$$\phi^S_t(\vec{x},t) \to 0 \quad t \to -\infty \tag{2.26}$$

In deriving the integral equation for the scattered potential, we choose the time dependent Green function derived by Wehausen and Laitone [23]

$$G(\vec{x};\vec{\xi},t-\tau) = G^{(0)}(\vec{x};\vec{\xi},t-\tau) + G^{(f)}(\vec{x};\vec{\xi},t-\tau) \tag{2.27}$$

$$G^{(0)}(\vec{x};\vec{\xi},t-\tau) = \frac{1}{r} - \frac{1}{r'} \tag{2.28}$$

$$G^{(f)}(\vec{x};\vec{\xi},t-\tau) = 2\int_0^\infty dk[1 - cos\sqrt{gk}\,(t-\tau)]e^{k(z+\zeta)}J_0(kR) \tag{2.29}$$

where:

$$\left.\begin{matrix} r \\ r' \end{matrix}\right\} \;=\; [(x-\xi)^2 \;+\; (y-\eta)^2 \;+\; (z \pm \zeta)^2]^{\frac{1}{2}}$$

$$R \;=\; (x-\xi)^2 \;+\; (y-\eta)^2. \tag{2.30}$$

We begin formulation of the integral equation by applying Green's second identity to $\phi^S_\tau(\vec{x},\tau)$ and $G(\vec{x};\vec{\xi},t-\tau)$:

$$\begin{aligned} &\iiint_{V(\tau)} d\vec{\xi}\,[\phi^S_\tau(\vec{\xi},\tau)\nabla^2 G(\vec{x};\vec{\xi},t-\tau) \;-\; G(\vec{x};\vec{\xi},t-\tau)\nabla^2\phi^S(\vec{\xi},\tau)] \\ &= \iint_{S(\tau)} d\vec{\xi}\,[\phi^S_\tau(\vec{\xi},\tau)G_{n_\xi}(\vec{x};\vec{\xi},t-\tau) \;-\; G(\vec{x};\vec{\xi},t-\tau)\phi^S_{\tau n_\xi}(\vec{\xi},\tau)] \;=\; 0 \end{aligned} \tag{2.31}$$

where we describe the entire surface of integration by the sum of its parts:

$$S \;=\; S_B \;\cup\; S_F \;\cup\; S_\epsilon \;\cup\; S_\infty.$$

We may may simplify the surface integral expression if we make note of the fact that

$$\iint_{S_\infty} [\cdots] \;\longrightarrow\; 0$$

$$\iint_{S_\epsilon} [\cdots] \;=\; 2\pi\phi^S_\tau(\vec{\xi},\tau).$$

The former expression is true by virtue of both the boundary conditions for the potential on S_∞ and the nature of the Green function, which as stated earlier, satisfies all problem boundary conditions except that for the body. We obtain latter expression since the point of the singularity is given on the body [19]. Given substitution for the

above surfaces, we may write the integral in the form:

$$2\pi\phi_\tau^S(\vec{\xi},\tau) + \iint_{S_b(t)} d\vec{\xi}\,[\phi_\tau^S(\vec{\xi},\tau)G_{n_\xi}(\vec{x};\vec{\xi},t-\tau) - \phi_{\tau n_\xi}^S(\vec{\xi},\tau)G(\vec{x};\vec{\xi},t-\tau)] + \iint_{S_f} d\vec{\xi}\,[\phi_\tau^S(\vec{\xi},\tau)G_{n_\xi}(\vec{x};\vec{\xi},t-\tau) - \phi_{\tau n_\xi}^S(\vec{\xi},\tau)G(\vec{x};\vec{\xi},t-\tau)] = 0. \quad (2.32)$$

In order to obtain an equation for the scattered potential itself and not its time derivative, we integrate by parts over time from $-\infty$ to t

$$2\pi\phi^S(t) + \iint_{S_b(t)} d\vec{\xi}\,[\phi^S(t)G_n(0) - G(0)\phi_n^S(t)] - \int_{-\infty}^{t} d\tau \iint_{S_b} d\vec{\xi}\,[\phi^S G_{\tau n} - \phi_n^S G_\tau] + \iint_{S_f} d\vec{\xi}\,[\phi^S(t)G_n(0)] - \int_{-\infty}^{t} d\tau \iint_{S_f} d\vec{\xi}\,[\phi^S G_{\tau n} - \phi_n^S G_\tau] = 0. \quad (2.33)$$

We would like to eliminate integration over the free surface, so we begin by substituting the free-surface boundary condition into equation 2.33:

$$2\pi\phi^S(t) + \iint_{S_b(t)} d\vec{\xi}\,[\phi^S(t)G_n(0) - G(0)\phi_n^S(t)] - \int_{-\infty}^{t} d\tau \iint_{S_b} d\vec{\xi}\,[\phi^S G_{\tau n} - \phi_n^S G_\tau] + \iint_{S_f} d\vec{\xi}\,[\phi^S(t)G_n(0)] + \frac{1}{g}\int_{-\infty}^{t} d\tau \iint_{S_f} d\vec{\xi}\,\{\phi^S[G_{\tau\tau\tau} - 2UG_{\tau\tau\xi} + U^2 G_{\tau\xi\xi}] - G_\tau[\phi_{\tau\tau}^S - 2U\phi_{\tau\xi}^S + U^2\phi_{\xi\xi}^S]\} = 0. \quad (2.34)$$

Integration by parts in time of the first bracketed expression in the free-surface integral yields

$$2\pi\phi^S(t) + \iint_{S_b(t)} d\vec{\xi}\,[\phi^S(t)G_n(0) - G(0)\phi_n^S(t)]$$

$$- \int_{-\infty}^{t} d\tau \iint_{S_b} d\vec{\xi} \, [\phi^S G_{\tau n} - \phi_n^S G_\tau]$$

$$+ \frac{U}{g} \int_{-\infty}^{t} d\tau \iint_{S_f} d\vec{\xi} \, [2\phi_\tau^S G_{\tau\xi} + 2\phi_{\tau\xi}^S G_\tau + U\phi^S G_{\tau\xi\xi} - U\phi_{\xi\xi}^S G_\tau] = 0. \quad (2.35)$$

Lastly, we may apply Stoke's theorem to the free-surface integral and reduce it to a contour integral over the waterline Γ to obtain the final equation

$$2\pi\phi^S(t) + \iint_{S_b} d\vec{\xi} \, \phi^S(t) G_n^{(0)} + \int_{-\infty}^{t} d\tau \iint_{S_b} d\vec{\xi} \, \phi^S G_{tn}^{(f)}$$

$$- \frac{U_o}{g} \int_{-\infty}^{t} d\tau \int_\Gamma n_1 dl [G_t^{(f)} \left(2\phi_\tau^S - U_o \phi_\xi^S\right) + U_o \phi^S G_{t\xi}^{(f)}]$$

$$= - \iint_{S_b} d\vec{\xi} \, G^{(0)} \phi_n^I(t) - \int_{-\infty}^{t} d\tau \iint_{S_b} d\vec{\xi} \, \phi_n^I G_t^{(f)} \quad (2.36)$$

where we have substituted:

$$G_t = -G_\tau$$

$$\phi_n^S = -\phi_n^I.$$

2.4 Diffraction Potential Formulation

Should we wish, we may also solve for the diffraction potential directly. In order to do so, we must first derive an integral equation for the incident potential $\phi^I(\vec{x}, t)$ which is a solution to the interior problem, that is, valid inside the body in the volume $\hat{V}$. We may then use this expression along with the previous expression derived for the scattered potential to get an integral equation for the diffraction potential. This method has been outlined in [12].

In the body interior, $\phi^I(\vec{x}, t)$ must satisfy Laplace's equation

$$\nabla^2 \phi^I(\vec{x}, t) = 0 \qquad \text{in } \hat{V} \quad (2.37)$$

as well as the boundary conditions

$$\left(\frac{\partial}{\partial t} - U\frac{\partial}{\partial x}\right)^2 \phi^I + g\frac{\partial \phi^I}{\partial z} = 0 \qquad \text{on } \hat{S}_F \tag{2.38}$$

$$\vec{n}\cdot\vec{\nabla}\phi^I = \vec{n}\cdot\vec{\nabla}\phi^S \qquad \text{on } S_B \tag{2.39}$$

and initial conditions

$$\phi^I(\vec{x},t) \to 0 \qquad \text{as } t \to -\infty \tag{2.40}$$

$$\phi^I_t(\vec{x},t) \to 0 \qquad \text{as } t \to -\infty \tag{2.41}$$

If we now solve for the incident potential in a manner similar to that which we used in the previous section, we obtain

$$\begin{aligned} &2\pi\phi^I(t) - \iint_{S_b} d\vec{\xi}\,\phi^I(t)G_n^{(0)} - \int_{-\infty}^{t} d\tau \iint_{S_b} d\vec{\xi}\,\phi^I G_{tn}^{(f)} \\ &+ \frac{U}{g}\int_{-\infty}^{t} d\tau \int_\Gamma n_1 dl[G_t^{(f)}\left(2\phi_\tau^I - U\phi_\xi^I\right) + U\phi^I G_{t\xi}^{(f)}] \\ &= -\iint_{S_b} d\vec{\xi}\,G^{(0)}\phi_n^I(t) - \int_{-\infty}^{t} d\tau \iint_{S_b} d\vec{\xi}\,\phi_n^I G_t^{(f)} \end{aligned} \tag{2.42}$$

Subtracting this from the expression for the scattered potential leads to the integral expression for the diffraction potential

$$\begin{aligned} &2\pi\phi^D(t) + \iint_{S_b} d\vec{\xi}\,\phi^D(t)G_n^{(0)} \\ &- \frac{U}{g}\int_{-\infty}^{t} d\tau \int_\Gamma n_1 dl[G_t^{(f)}\left(2\phi_\tau^D - U\phi_\xi^D\right) + U\phi^D G_{t\xi}^{(f)}] \\ &= 4\pi\phi^I - \int_{-\infty}^{t} d\tau \iint_{S_b} d\vec{\xi}\,\phi^D G_{tn}^{(f)} \end{aligned} \tag{2.43}$$

2.5 The Impulse-Response Function

The most interesting quantities we may obtain by solving for the diffraction potential, using either equation (2.36) or (2.43), are the forces on the body created by the incident and scattered waves. As shown in [3], it is convenient to represent these forces in terms of impulse-response functions. In so doing, we are able to predict the exciting force response given any arbtrary incident wave elevation.

We begin by defining the pressure over the body. The pressure due to the diffraction potential can be determined from the linearized Bernoulli equation:

$$p = -\rho\left(\frac{\partial\phi^D}{\partial t} + \vec{\nabla}\bar{\Phi}\cdot\vec{\nabla}\phi^D\right). \tag{2.44}$$

We may therefore describe the related forces as the integral of the pressure over the body

$$F_j = -\rho\iint_{S_b} d\vec{\xi}\left(\frac{\partial\phi^D}{\partial t} + \vec{\nabla}\bar{\Phi}\cdot\vec{\nabla}\phi^D\right)n_j, \tag{2.45}$$

where n_j represent the components of the normal vector for the rigid-body modes of motion as defined in equation (2.18). This expression is inconvenient, however, since it requires that we know the gradients of the potentials as well as the potentials themselves. We may alleviate this concern by applying Tuck's theorem, i.e.,

$$\iint_{S_b} d\vec{\xi}\,[m_j\phi^D + n_j(\vec{\nabla}\bar{\Phi}\cdot\vec{\nabla}\phi^D)] = -\int_\Gamma dl\phi^D n_j(\vec{l}\times\vec{n})\cdot\vec{\nabla}\bar{\Phi}, \tag{2.46}$$

where m_j represents the m-terms as defined in equation (2.19). Substitution of (2.46) into (2.45) yields

$$F_j = -\rho \iint_{S_b} d\vec{\xi} \left(\frac{\partial \phi^D}{\partial t} n_j - \phi^D m_j \right)$$

$$+\rho \int_\Gamma dl \phi^D n_j (\vec{l} \times \vec{n}_{2D}) \cdot \vec{\nabla} \bar{\Phi}. \tag{2.47}$$

Given that we may define the time dependent exciting forces by a convolution of an impulse-response function and arbitrary input wave elevation

$$X_j = \int_{-\infty}^{\infty} d\tau K_{jD}(t-\tau)\zeta(\tau), \tag{2.48}$$

and we may define similar expressions for the diffraction potential and its time derivative (see [5]), the impulse response function representing the exciting forces can be given as:

$$K_{jD}(t) = -\rho \left[\iint_{S_b} d\vec{\xi} \frac{\partial \phi^D}{\partial t} n_j - \iint_{S_b} d\vec{\xi}\, \phi^D m_j - \int_\Gamma dl \phi^D n_j (\vec{l} \times \vec{n}) \cdot \vec{\nabla} \bar{\Phi} \right]. \tag{2.49}$$

We may assume that the waterline term is negligible if the vessel is thin and wall-sided.

2.6 The Forward Speed Haskind Relations in the Time Domain

In order to determine the exciting forces due to the scattered and incident potentials in the ship motions problem, it has been shown that for zero forward speed, the Haskind relations are quite useful in both the frequency domain [15] and time domain [22]. For the zero speed problem in the time domain, Wehausen was able to obtain the expression

$$X_i(t) = \iint_{S_b} d\vec{\xi}\,[\phi^I_{nt}(\vec{\xi},t)\phi_i(\vec{\xi},0) - \phi^I_t(\vec{\xi},t)\phi_{in}(\vec{\xi},0)]$$

$$+ \int_0^\infty d\tau \iint_{S_b} d\vec{\xi}\,\phi^I_{nt}(\vec{\xi},t)\phi_{it}(\vec{\xi},t-\tau), \tag{2.50}$$

where $\phi_i(\vec{x},t)$ is the solution for the radiation problem in mode of motion i. We can see the advantages of using this form to obtain the exciting forces. If we were concerned with many incident wave headings and used the scattered potential formulation, we would have to solve as many scattered problems as there are wave headings. On the other hand, if we use equation (2.50), we must only solve one radiation problem. It would be nice, then, if there could be found analogous expressions for the forward speed problem. The case of forward speed Haskind relations in the frequency domain has been discussed in [16]. As opposed to the zero speed case, where the forward flow radiation potential was used as assisting potential, here it is necessary to employ the reverse flow radiation potential instead. In turning our attention to the forward speed case in the time domain, we shall find the same to hold true.

We begin by defining the exciting force due to the scattered potential of a body moving with steady forward speed as:

$$X_i(t) = -\rho \iint_{S_b} d\vec{\xi}\,[\phi^S_t(\vec{\xi},t) + \vec{\nabla}\bar{\Phi}(\vec{\xi})\cdot\vec{\nabla}\phi^S(\vec{\xi},t)]n_i \tag{2.51}$$

where $\vec{\nabla}\bar{\Phi}$ is the velocity vector due to the steady potential. In order to obtain an expression corresponding to $X_i(t)$, we will make use of Green's second identity with the scattered potential $\phi^S(\vec{x},t)$ and the reverse flow radiation potential $\phi^-_k(\vec{x},t-\tau)$ as the assisting potential. These potentials must satisfy the conditions set forth for their respective boundary value problems in the moving coordinate system. For the scattered potential, we have the familiar boundary conditions:

$$\nabla^2\phi^S(\vec{x},t) = 0 \qquad \text{in } V \tag{2.52}$$

$$(\frac{\partial}{\partial t} - U_o\frac{\partial}{\partial x})^2\phi^S + g\frac{\partial}{\partial z}\phi^S = 0 \qquad \text{on } S_F, \tag{2.53}$$

$$\vec{n}\cdot\vec{\nabla}\phi^S = -\vec{n}\cdot\vec{\nabla}\phi^I \qquad \text{on } S_B, \tag{2.54}$$

and

$$\vec{\nabla}\phi^S \to 0 \qquad \text{on } S_\infty \text{ for } t \text{ finite.} \tag{2.55}$$

The reverse flow radiation potentials must satisfy a different boundary condition on the body and are described by:

$$\nabla^2\phi_k^-(\vec{x}, t-\tau) = 0 \qquad \text{in } V \tag{2.56}$$

$$(\frac{\partial}{\partial t} + U_o\frac{\partial}{\partial x})^2\phi_k^- + g\frac{\partial}{\partial z}\phi_k^- = 0 \qquad \text{on } S_F, \tag{2.57}$$

$$\vec{n}\cdot\vec{\nabla}\phi_k^- = n_k\dot{\alpha}_k - m_k\alpha_k \qquad \text{on } S_B, \tag{2.58}$$

$$\phi_k^- \to 0 \qquad \text{on } S_\infty \text{ for } t \text{ finite,} \tag{2.59}$$

and

$$\vec{\nabla}\phi_k^- \to 0 \qquad \text{on } S_\infty \text{ for } t \text{ finite.} \tag{2.60}$$

As seen before, we require two initial conditions for this problem which are

$$\phi^S(\vec{x}, t) \to 0 \qquad \text{on } z = 0, t \to -\infty \tag{2.61}$$

and

$$\phi_i^S(\vec{x}, t) \to 0 \qquad \text{on } z = 0, t \to -\infty. \tag{2.62}$$

Application of Green's second identity yields:

$$\iiint_{V(\tau)} d\vec{\xi}\,[\phi_\tau^S(\vec{\xi},\tau)\nabla^2\phi_k^-(\vec{\xi},t-\tau) - \phi_k^-(\vec{\xi},t-\tau)\nabla^2\phi_\tau^S(\vec{\xi},\tau)]$$
$$= \iint_{S(\tau)} d\vec{\xi}\,[\phi_\tau^S(\vec{\xi},\tau)\phi_{kn}^-(\vec{\xi},t-\tau) - \phi_{\tau n}^S(\vec{\xi},\tau)\phi_k^-(\vec{\xi},t-\tau)] = 0 \qquad (2.63)$$

Therefore, we are able to construct the boundary value integral equation:

$$\iint_{S_b} d\vec{\xi}\,[\phi_\tau^S(\vec{\xi},\tau)\phi_{kn}^-(\vec{\xi},t-\tau) - \phi_{\tau n}^S(\vec{\xi},\tau)\phi_k^-(\vec{\xi},t-\tau)]$$
$$+ \iint_{S_f} d\vec{\xi}\,[\phi_\tau^S(\vec{\xi},\tau)\phi_{kn}^-(\vec{\xi},t-\tau) - \phi_{\tau n}^S(\vec{\xi},\tau)\phi_k^-(\vec{\xi},t-\tau)]$$
$$+ \iint_{S_\infty} d\vec{\xi}\,[\phi_\tau^S(\vec{\xi},\tau)\phi_{kn}^-(\vec{\xi},t-\tau) - \phi_{\tau n}^S(\vec{\xi},\tau)\phi_k^-(\vec{\xi},t-\tau)] = 0 \qquad (2.64)$$

The integral over S_∞ gives no contribution since ϕ_n^S and ϕ_n^- approach zero as $R \to \infty$. We now integrate over time from $-\infty$ to t to yield

$$\int_{-\infty}^{t} d\tau \iint_{S_b} d\vec{\xi}\,[\phi_\tau^S(\vec{\xi},\tau)\phi_{kn}^-(\vec{\xi},t-\tau) - \phi_{\tau n}^S(\vec{\xi},\tau)\phi_k^-(\vec{\xi},t-\tau)]$$
$$+ \int_{-\infty}^{t} d\tau \iint_{S_f} d\vec{\xi}\,[\phi_\tau^S(\vec{\xi},\tau)\phi_{kn}^-(\vec{\xi},t-\tau) - \phi_{\tau n}^S(\vec{\xi},\tau)\phi_k^-(\vec{\xi},t-\tau)] = 0 \qquad (2.65)$$

If we integrate the body surface term by parts and substitute the free surface boundary condition (noting carefully that $\frac{\partial\phi_k^-}{\partial\tau} = -\frac{\partial\phi_k^-}{\partial t}$) we arrive at the expression

$$\iint_{S_b} d\vec{\xi}\,\phi^S(\vec{\xi},t)\phi_{kn}^-(0) - \int_{-\infty}^{t} d\tau \iint_{S_b} d\vec{\xi}\,[\phi^S(\vec{\xi},\tau)\phi_{k\tau n}^-(\vec{\xi},t-\tau)]$$
$$- \iint_{S_b} d\vec{\xi}\,\phi_n^S(\vec{\xi},t)\phi_k^-(0) + \int_{-\infty}^{t} d\tau \iint_{S_b} d\vec{\xi}\,[\phi_n^S(\vec{\xi},\tau)\phi_{k\tau}^-(\vec{\xi},t-\tau)]$$
$$-\frac{1}{g}\int_{-\infty}^{t} d\tau \iint_{S_f} d\vec{\xi}\,[\phi_\tau^S(\vec{\xi},\tau)[\phi_{k\tau\tau}^-(\vec{\xi},t-\tau) - 2U_o\phi_{k\tau\xi}^-(\vec{\xi},t-\tau) + U_o^2\phi_{k\xi\xi}^-(\vec{\xi},t-\tau)]$$
$$-\phi_k^-(\vec{\xi},t-\tau)[\phi_{\tau\tau\tau}^S(\vec{\xi},\tau) - 2U_o\phi_{\tau\tau\xi}^S(\vec{\xi},\tau) + U_o^2\phi_{\tau\xi\xi}^S(\vec{\xi},\tau)]] = 0 \qquad (2.66)$$

Let's consider only the free surface term for a moment. Separating terms by factor of forward speed we find

$$I_{S_f} = -\frac{1}{g}\int_{-\infty}^{t} d\tau \iint_{S_f} d\vec{\xi}\,[\phi_\tau^S(\vec{\xi},\tau)\phi^-_{k\tau\tau}(\vec{\xi},t-\tau) - \phi^-_k(\vec{\xi},t-\tau)\phi^S_{\tau\tau\tau}(\vec{\xi},\tau)]$$
$$-\frac{2U_o}{g}\int_{-\infty}^{t} d\tau \iint_{S_f} d\vec{\xi}\,[-\phi_\tau^S(\vec{\xi},\tau)\phi^-_{k\tau\xi}(\vec{\xi},t-\tau) + \phi^-_k(\vec{\xi},t-\tau)\phi^S_{\tau\tau\xi}(\vec{\xi},\tau)]$$
$$-\frac{U_o^2}{g}\int_{-\infty}^{t} d\tau \iint_{S_f} d\vec{\xi}\,[\phi_\tau^S(\vec{\xi},\tau)\phi^-_{k\xi\xi}(\vec{\xi},t-\tau) - \phi^-_k(\vec{\xi},t-\tau)\phi^S_{\tau\xi\xi}(\vec{\xi},\tau)] \qquad (2.67)$$

If we integrate the second half of the first term on the right hand side by parts, we may rewrite this part of the free surface integral as

$$-\frac{1}{g}\int_{-\infty}^{t} d\tau \iint_{S_f} d\vec{\xi}\,\frac{\partial}{\partial\tau}[\phi_\tau^S(\vec{\xi},\tau)\phi^-_{k\tau}(\vec{\xi},t-\tau)] \qquad (2.68)$$

which is identically zero due to the initial conditions of the boundary value problem. Recombining the right hand side gives

$$I_{S_f} = -\frac{1}{g}\int_{-\infty}^{t} d\tau \iint_{S_f} d\vec{\xi}\,[\phi_\tau^S(\vec{\xi},\tau)[-2U_o\phi^-_{k\tau\xi}(\vec{\xi},t-\tau) + U_o^2\phi^-_{k\xi\xi}(\vec{\xi},t-\tau)]$$
$$+\phi^-_k(\vec{\xi},t-\tau)[2U_o\phi^S_{\tau\tau\xi}(\vec{\xi},\tau) + U_o^2\phi^S_{\tau\xi\xi}(\vec{\xi},\tau)]] \qquad (2.69)$$

We now integrate the second term on the right hand side by parts in order to get the integrand of the free surface integral as a partial derivative with respect to ξ

$$I_{S_f} = -\frac{1}{g}\int_{-\infty}^{t} d\tau \iint_{S_f} d\vec{\xi}\,[\phi_\tau^S(\vec{\xi},\tau)[-2U_o\phi^-_{k\tau\xi}(\vec{\xi},t-\tau) + U_o^2\phi^-_{k\xi\xi}(\vec{\xi},t-\tau)]$$
$$-\phi^-_{k\tau}(\vec{\xi},t-\tau)[2U_o\phi^S_{\tau\xi}(\vec{\xi},\tau) + U_o^2\phi^S_{\xi\xi}(\vec{\xi},\tau)]]$$

$$= \frac{1}{g}\int_{-\infty}^{t} d\tau \iint_{S_f} d\vec{\xi}\,\frac{\partial}{\partial\xi}[\phi_\tau^S(\vec{\xi},\tau)[U_o\phi^-_{k\tau}(\vec{\xi},t-\tau) - U_o^2\phi^-_{k\xi}(\vec{\xi},t-\tau)]$$

$$+\phi^-_{k\tau}(\vec{\xi},t-\tau)[U_o\phi^S_\tau(\vec{\xi},\tau)-U_o^2\phi^S_\xi(\vec{\xi},\tau)]] \tag{2.70}$$

and so we may move the integral over the free surface to one over the waterlines Γ and Γ_∞

$$\begin{aligned} I_{S_f} = \frac{1}{g}\int_{-\infty}^{t} d\tau \int_{\Gamma\cup\Gamma_\infty} d\eta\ [\phi^S_\tau(\vec{\xi},\tau)[U_o\phi^-_{k\tau}(\vec{\xi},t-\tau)-U_o^2\phi^-_{k\xi}(\vec{\xi},t-\tau)] \\ +\phi^-_{k\tau}(\vec{\xi},t-\tau)[U_o\phi^S_\tau(\vec{\xi},\tau)-U_o^2\phi^S_\xi(\vec{\xi},\tau)]] \end{aligned} \tag{2.71}$$

Once again, the integral over Γ_∞ gives no contribution. Substituting the waterline integral, the full integral equation becomes:

$$\begin{aligned} &\iint_{S_b} d\vec{\xi}\ \phi^S(\vec{\xi},t)\phi^-_{kn}(0)+\int_{-\infty}^{t} d\tau \iint_{S_b} d\vec{\xi}\ [\phi^S(\vec{\xi},\tau)\phi^-_{ktn}(\vec{\xi},t-\tau)] \\ &=\iint_{S_b} d\vec{\xi}\ \phi^S_n(\vec{\xi},t)\phi^-_k(0)+\int_{-\infty}^{t} d\tau \iint_{S_b} d\vec{\xi}\ [\phi^S_n(\vec{\xi},\tau)\phi^-_{kt}(\vec{\xi},t-\tau)] \\ &+\frac{1}{g}\int_{-\infty}^{t} d\tau \int_{\Gamma} d\eta\ [\phi^S_t(\vec{\xi},\tau)[U_o\phi^-_{kt}(\vec{\xi},t-\tau)+U_o^2\phi^-_{k\xi}(\vec{\xi},t-\tau)] \\ &\qquad +\phi^-_{kt}(\vec{\xi},t-\tau)[U_o\phi^S_t(\vec{\xi},\tau)-U_o^2\phi^S_\xi(\vec{\xi},\tau)]] \end{aligned} \tag{2.72}$$

where we have substituted partial derivatives with respect to τ with partial derivatives with respect to t. Imposing the body boundary condition for the reverse flow radiation potential we find

$$\begin{aligned} &\iint_{S_b} d\vec{\xi}\ \phi^S(\vec{\xi},t)n_k-\int_{-\infty}^{t} d\tau \iint_{S_b} d\vec{\xi}\ [\phi^S(\vec{\xi},\tau)m_k] \\ &=\iint_{S_b} d\vec{\xi}\ \phi^S_n(\vec{\xi},t)\phi^-_k(0)+\int_{-\infty}^{t} d\tau \iint_{S_b} d\vec{\xi}\ [\phi^S_n(\vec{\xi},\tau)\phi^-_{kt}(\vec{\xi},t-\tau)] \\ &+\frac{1}{g}\int_{-\infty}^{t} d\tau \int_{\Gamma} d\eta\ [\phi^S_t(\vec{\xi},\tau)[U_o\phi^-_{kt}(\vec{\xi},t-\tau)+U_o^2\phi^-_{k\xi}(\vec{\xi},t-\tau)] \\ &\qquad +\phi^-_{kt}(\vec{\xi},t-\tau)[U_o\phi^S_t(\vec{\xi},\tau)-U_o^2\phi^S_\xi(\vec{\xi},\tau)]] \end{aligned} \tag{2.73}$$

Now we may employ Tuck's theorem [18] which, as applied to our case, states

$$\iint_{S_b} d\vec{\xi}\, \phi^S m_k = -\iint_{S_b} d\vec{\xi}\, (\vec{\nabla}\bar{\Phi}\cdot\vec{\nabla}\phi^S) n_k - \int_\Gamma dl\, \phi^S n_k (\vec{l}\times\vec{n}_{2D})\cdot\vec{\nabla}\bar{\Phi} \tag{2.74}$$

If we make the assumption that the body is slender, the waterline integral is of higher order than the surface integrals and so is negligible. We substitute this expression as well as the body boundary condition for the scattered potential into the integral equation to obtain

$$\begin{aligned}
&\iint_{S_b} d\vec{\xi}\, \phi^S(\vec{\xi},t) n_k + \int_{-\infty}^{t} d\tau \iint_{S_b} d\vec{\xi}\, [\vec{\nabla}\bar{\Phi}\cdot\vec{\nabla}\phi^S(\vec{\xi},\tau)] n_k \\
&= -\iint_{S_b} d\vec{\xi}\, \phi_n^I(\vec{\xi},t)\phi_k^-(0) - \int_{-\infty}^{t} d\tau \iint_{S_b} d\vec{\xi}\, [\phi_n^I(\vec{\xi},\tau)\phi_{kt}^-(\vec{\xi},t-\tau)] \\
&\quad + \frac{1}{g}\int_{-\infty}^{t} d\tau \int_\Gamma d\eta\, [\phi_t^S(\vec{\xi},\tau)[U_o\phi_{kt}^-(\vec{\xi},t-\tau) + U_o^2\phi_{k\xi}^-(\vec{\xi},t-\tau)] \\
&\quad + \phi_{kt}^-(\vec{\xi},t-\tau)[U_o\phi_t^S(\vec{\xi},\tau) - U_o^2\phi_\xi^S(\vec{\xi},\tau)]]
\end{aligned} \tag{2.75}$$

At this point, we should make a few comments regarding the use of the reverse flow radiation potential. We can see that this choice of assisting potential has helped us not only to obtain the correct term for the left hand side of our expression but also to move the free surface integral to the waterline. The former is accomplished by providing a suitable body boundary condition for the radiation potential. The latter is accomplished by virtue of the free surface condition. Similar results can be seen from the treatment of the frequency domain problem in [16]. If we once again assume a slender body, the integral over the waterline is small and neglible. We now take a derivitive of the expression with respect to time

$$\begin{aligned}
&\iint_{S_b} d\vec{\xi}\, [\phi_t^S(\vec{\xi},t) + \vec{\nabla}\bar{\Phi}\cdot\vec{\nabla}\phi^S(\vec{\xi},\tau)] n_k \\
&= -\iint_{S_b} d\vec{\xi}\, \phi_{tn}^I(\vec{\xi},t)\phi_k^-(0) - \int_{-\infty}^{t} d\tau \iint_{S_b} d\vec{\xi}\, [\phi_{tn}^I(\vec{\xi},\tau)\phi_{kt}^-(\vec{\xi},t-\tau)],
\end{aligned} \tag{2.76}$$

and finally on making the substitution:

$$\phi_t^S = \phi_t^D - \phi_t^I$$
$$\vec{\nabla}\phi^S = \vec{\nabla}\phi^D - \vec{\nabla}\phi^I,$$

we obtain the expression for the exciting force as:

$$\begin{aligned} X_i(t) &= -\iint_{S_b} d\vec{\xi}\,[\phi_t^S(\vec{\xi},t) + \vec{\nabla}\bar{\Phi}\cdot\vec{\nabla}\phi^S(\vec{\xi},\tau)]n_k \\ &= -[\phi_t^S(\vec{\xi},t) + \vec{\nabla}\bar{\Phi}\cdot\vec{\nabla}\phi^S(\vec{\xi},\tau)]n_k + \iint_{S_b} d\vec{\xi}\,\phi_{tn}^I(\vec{\xi},t)\phi_k^-(0) \\ &\quad + \int_{-\infty}^{t} d\tau \iint_{S_b} d\vec{\xi}\,[\phi_{tn}^I(\vec{\xi},\tau)\phi_{kt}^-(\vec{\xi},t-\tau)], \end{aligned} \tag{2.77}$$

which is equivalent to (2.50) when the body is stationary.

2.7 Special Case: Following Seas

The general expression for the linear system response due to an impulsive incident wave field may be written as

$$X(t) = \int_{-\infty}^{\infty} K(t-\tau)\zeta(\tau)d\tau \tag{2.78}$$

where $K(t)$ is the impulse response function corresponding to the incident wave field given by the potential found in King [11]

$$\phi^I(\vec{x},t) = \frac{1}{\pi}\int_{-\infty}^{\infty} d\omega_e \frac{ig}{\omega} e^{\left[kz - ik[(x\cos\beta + y\sin\beta] + i\omega_e t\right]} \tag{2.79}$$

and $\zeta(t)$ is the input wave elevation taken in the ship-fixed coordinate system. In general, $\zeta(t)$ may be given in terms of the more readily available information in

the inertial coordinate system if we consider the following convolution using a time-varying kernel as shown in King [11]:

$$\zeta(t) = \int_{-\infty}^{+\infty} h(t-\tau,\tau)\zeta_o(\tau)d\tau. \tag{2.80}$$

Substitution of $\zeta(t) = e^{(i\omega t)}$ leads to the impulse response function

$$h(t-\tau,\tau) = \Re\Big\{\frac{1}{\pi}\int_0^{\infty} e^{(-ikU\cos\beta\tau)}e^{(i\omega t)}e^{(-i\omega\tau)}d\omega\Big\} \tag{2.81}$$

and using the properties of convolution produces

$$\zeta(t) = \Re\Big\{\frac{1}{\pi}\int_0^{\infty} d\omega_e \frac{\bar{\zeta}(\omega)}{1-\frac{2U\omega\cos\beta}{g}}e^{(i\omega_e t)}\Big\} \tag{2.82}$$

where $\bar{\zeta}(\omega)$ is the frequency dependent wave elevation input in the inertial coordinate system and we have substituted

$$d\omega_e = (1 - \frac{2U\omega\cos\beta}{g})d\omega \tag{2.83}$$

which we may obtain from the relation

$$\omega_e = \omega - \frac{U\omega^2\cos\beta}{g} \tag{2.84}$$

We now turn our attention to the specific case of following seas. When we consider the wave elevation in following seas as measured from the ship-fixed coordinate system, we realize that there will be an ambiguity when we try to resolve this input in terms of its absolute frequency. The reason for this ambiguity is that there are two

wavelengths apparently overtaking the ship and one which the ship is overtaking, yet all three wavelengths have the same encounter frequency. If we are measuring wave elevation from the ship-fixed system, we have no way of distinguishing between the three different wavelengths. We may reconcile this situation by considering the input in three separate parts which fall in the restricted range of wavelengths:

$$\begin{aligned} 0 < k_1 &< \frac{g}{4U^2\cos^2\beta} \\ \frac{g}{4U^2\cos^2\beta} < k_2 &< \frac{g}{U^2\cos^2\beta} \\ \frac{g}{U^2\cos^2\beta} < k_3 &< \infty \end{aligned}$$

It is interesting to note how waves in each of the three groups appear to the ship and where the wave groups are positioned with respect to the ship. Given the definition

$$\tau = \frac{\omega_e U}{g} = \kappa - \sqrt{|\kappa|} \tag{2.85}$$

where κ is the ratio of wave number to the wave number of waves with phase speed $U\cos\beta$. For the case of three-dimensional waves we can define κ as

$$\kappa = \frac{kU^2\cos^2\beta}{g}. \tag{2.86}$$

Then we have $\tau = 0$ at $k = 0$ and $k = \frac{g}{U^2\cos^2\beta}$, $|\tau| < 1$ for $k < \frac{g}{U^2\cos^2\beta}$, and $|\tau| = \frac{1}{4}$ at $k = \frac{g}{4U^2\cos^2\beta}$. Thus, we may relate κ to both the phase velocity and group velocity of the waves:

$$\frac{v_p}{U} = \frac{1}{\sqrt{\kappa}} \tag{2.87}$$

$$\frac{v_g}{U} = \frac{1}{2\sqrt{\kappa}} \tag{2.88}$$

We see, then, for the range of k_1, $0 < \kappa < \frac{1}{4}$, and so the phase velocity and group velocity of these waves are always greater than the ship velocity. For the range of k_2, $\frac{1}{4} < \kappa < 1$, and so while the phase velocity of these waves will be greater than the ship velocity, their group velocity will be less than the ship velocity. Finally, for the range of k_3, $\kappa < 1$, and so both the phase and group velocity of these waves will be less than the ship velocity.

Given the ambiguity in absolute frequency, we find a need for three separate impulse response functions and thus must modify our force convolution equation accordingly:

$$X(t) = \sum_{m=1}^{3} \int_{-\infty}^{\infty} K_m(t-\tau)\zeta_m(\tau)d\tau \tag{2.89}$$

where now the wave elevation in the ship-fixed frame is given by

$$\zeta_m(t) = \Re\Big\{\frac{1}{\pi}\int_0^{g/4U\cos\beta} \frac{\bar{\zeta}(\omega_m)}{1-\frac{2U\omega_m\cos\beta}{g}} e^{(i\omega_e t)} d\omega_e\Big\} \quad m = 1,2 \tag{2.90}$$

$$= \Re\Big\{\frac{1}{\pi}\int_0^{\infty} \frac{\bar{\zeta}(\omega_m)}{1-\frac{2U\omega_m\cos\beta}{g}} e^{(-i\omega_e t)} d\omega_e\Big\} \quad m = 3 \tag{2.91}$$

Likewise, we may obtain three separate impulse-response function representations for $\nabla\phi^I(\vec{x},t)$ and $\phi_t^I(\vec{x},t)$. These may be given by the form found in [11]:

$$\vec{\nabla}\phi_m^I(\vec{x},t) = \frac{1}{\pi}\Re\Big\{\begin{bmatrix}\hat{i}\cos\beta\\ \hat{j}\sin\beta\\ \hat{k}i\end{bmatrix}\int_0^{g/4U\cos\beta} \omega_m e^{\left[kz-ik[x\cos\beta+y\sin\beta]\right]} e^{(i\omega_e t)} d\omega_e\Big\}$$

$$\text{for } m = 1,2 \tag{2.92}$$

$$= \frac{1}{\pi}\Re\Big\{ \begin{bmatrix} \hat{i}\cos\beta \\ \hat{j}\sin\beta \\ \hat{k}i \end{bmatrix} \int_0^\infty \omega_m e^{\left[kz+ik[x\cos\beta+y\sin\beta]\right]} e^{(i\omega_e t)} d\omega_e \Big\}$$

$$\text{for } m = 3 \tag{2.93}$$

and

$$\phi^I_{mt}(\vec{x},t) = \frac{-g}{\pi}\Re\Big\{ \int_0^{g/4U\cos\beta} \frac{\omega_e}{\omega_m} e^{\left[kz-ik[x\cos\beta+y\sin\beta]\right]} e^{(i\omega_e t)} d\omega_e \Big\}$$

$$\text{for } m = 1,2 \tag{2.94}$$

$$= \frac{-g}{\pi}\Re\Big\{ \int_0^\infty \frac{\omega_e}{\omega_m} e^{\left[kz+ik[x\cos\beta+y\sin\beta]\right]} e^{(i\omega_e t)} d\omega_e \Big\}$$

$$\text{for } m = 3 \tag{2.95}$$

Finally, we can also express the frequency for each range as a function of encounter frequency

$$\omega_1 = \frac{g}{2U\cos\beta}\left(1 - \sqrt{1 - \frac{4U\cos\beta}{g}\omega_e}\right) \tag{2.96}$$

$$\omega_2 = \frac{g}{2U\cos\beta}\left(1 + \sqrt{1 - \frac{4U\cos\beta}{g}\omega_e}\right) \tag{2.97}$$

$$\omega_3 = \frac{g}{2U\cos\beta}\left(1 + \sqrt{1 + \frac{4U\cos\beta}{g}\omega_e}\right) \tag{2.98}$$

Chapter 3

Development of the Numerical Scheme

3.1 Panel Methods

Having laid out an analytical scheme for calculation of the velocity potential, we must now develop a numerical scheme which will solve equation (2.36). In order to do so, we must be able to approximate the surface of the body as well as numerically solve a Fredholm integral equation of the second kind. We can accomplish both tasks using a class of processes known as panel methods. In the case of the former task, we use a number of plane quadralateral elements (triangular elements when necessary) to describe the body surface. In the case of the latter task, we discretize the integral equation as a system of linear equations and solve it using standard matrix techniques such as LU-decomposition. This subsection will describe the general approach used in this numerical technique.

The pioneering effort in this area using an arbitrary three-dimensional body was presented by Hess and Smith [9]. The first step is to define the body by a set of points taken along its surface. The points are then grouped appropiately to form panels. Most often the panels are quadralaterals, however, occasionally triangular panels are used, especially in areas of high curvature. Likewise, areas of high curvature tend to necessitate a greater number of panels to produce accurate results. Determination of

the surface points depends upon the body being modelled. Generally when modelling a ship's surface, the only available information is from its lines drawings. In this case, the shape of the hull's cross section is known at a number of stations along the length of the ship. Such a method of choosing surface points is conceptually simple. In a few instances, however, it is possible to mathematically define the body (e.g. the Wigley hull form). This procedure is also quite useful in modelling bodies such as tension leg platforms or submarines.

At times, the four points describing a quadralateral are not coplanar. Two possible means of rectifying the problem can be using either triangular panels or the method described in [9]. An equivalent method is employed by T$\bar{\text{I}}$MIT . Here, vertices are connected using straight segments. The quadralateral plane is then defined by the midpoints of these segments with the original vertices projected onto this plane.

Once the body has been discretized, it is necessary to discretize the integral equation. We begin by assuming that the potential is constant over each panel and use the panel centroid as the collocation point. Thus for each panel j we can write the approximation

$$\phi = \phi_j$$

$$\frac{\partial \phi}{\partial n} = v_j.$$

If we have the general integral equation

$$2\pi\phi(\vec{x}) + \iint \phi(\vec{\xi})\frac{\partial}{\partial n_\xi}G(\vec{x};\vec{\xi})dS_\xi$$

$$= \iint G(\vec{x};\vec{\xi})\frac{\partial}{\partial n_\xi}\phi(\vec{\xi})dS_\xi, \tag{3.1}$$

then using the above approximations we can write it in its discrete form:

$$2\pi\phi_i + \sum_{j=1}^{N} \phi_j \iint \frac{\partial G}{\partial n_\xi} dS_\xi = \sum_{j=1}^{N} v_j \iint G dS \tag{3.2}$$

where N is the total number of panels describing the body and the surface integral is taken over the j^{th} panel.

3.2 Discretization of the Integral Equation

In the previous subsection, we saw the general form of the discretization of a Fredholm integral equation of the second kind. We now apply this method specifically to equation (2.36). In this case, we are dealing with a potential which is a function of both time and space so we must now work with discretization in two variables. Time discretization becomes a factor in computing the convolution integrals. These convolution terms are found only on the right-hand side and may be calculated using the trapazoidal rule. Keeping this in mind, we may determine the specific linear system

$$2\pi\phi_{iM} + \sum_{j=1}^{NP} \phi_{jM} \iint_{S_j} dS \frac{\partial G^{(0)}(\vec{x};\vec{\xi})}{\partial n_\xi} - \frac{U}{g} \sum_{j=1}^{NW} \phi_{jM} \int_{\Gamma_j} n_1 dl \left(\frac{\partial G^{(f)}(\vec{x};\vec{\xi})}{\partial t}\right)_1$$

$$= -\sum_{m=0}^{M-1} {}' \Delta t \sum_{j=1}^{NP} \left\{ \phi_{jm} \iint_{S_j} dS \left(\frac{\partial^2 G^{(f)}(\vec{x};\vec{\xi})}{\partial n_\xi \partial t}\right)_{M-m} - \left(\frac{\partial \phi}{\partial n_\xi}\right)_{jm} \iint_{S_j} dS \left(\frac{\partial G^{(f)}(\vec{x};\vec{\xi})}{\partial t}\right)_{M-m} \right\}$$

$$+ \sum_{j=1}^{NP} \left(\frac{\partial \phi}{\partial n_\xi}\right)_{jm} \iint_{S_j} dS G^{(0)}(\vec{x};\vec{\xi})$$

$$- \frac{U^2}{g} \sum_{m=1}^{M-1} \Delta t \sum_{j=1}^{NW} \left\{ \left(\frac{\partial \phi}{\partial \xi}\right)_{jm} \int_{\Gamma_j} n_1 dl \left(\frac{\partial G^{(f)}(\vec{x};\vec{\xi})}{\partial t}\right)_{M-m} - \phi_{jm} \int_{\Gamma_j} n_1 dl \left(\frac{\partial^2 G^{(f)}(\vec{x};\vec{\xi})}{\partial \xi \partial t}\right)_{M-m} \right\}$$

$$+ \frac{U}{g} \sum_{m=1}^{M-2} \sum_{j=1}^{NW} (\phi_{jm+1} - \phi_{jm-1}) \int_{\Gamma_j} n_1 dl \left(\frac{\partial G^{(f)}(\vec{x};\vec{\xi})}{\partial t}\right)_{M-m}$$

$$- \frac{U}{g} \sum_{j=1}^{NW} \phi_{jM-2} \int_{\Gamma_j} n_1 dl \left(\frac{\partial G^{(f)}(\vec{x};\vec{\xi})}{\partial t}\right)_1 \tag{3.3}$$

where S_j is the surface of the j^{th} panel, Γ_j is the waterline segment of the j^{th} panel, NP is the total number of panels used to describe the body, NW is the number of waterline panels on the body, and M is the total number of time steps [5]. The prime on the temporal summation is used to denote that a weight of one-half is applied when $m = 0$. Equation (3.3) represents an $NP \times NP$ linear system with NP unknowns for each time step.

One very nice property of this linear system of equations is that the matrix on the left-hand side need only be factored at two time steps, the first time step and the third time step. Investigation of equation (3.3) reveals why this is true. We first note that the coefficients of the left-hand side matrix are essentially time indepenedent. The key to needing two factorizations, then, lies in the use of a central difference scheme to determine the value of the time derivative of ϕ at the M-1 time step. We need this value to complete the convolution in the next to last term on the right-hand side of the equation (which in its present form only goes to the M-2 time step), but the central difference scheme used to find it introduces two extra terms. One term, of known quantities, is the last right-hand side expression. The other term involves the unknown ϕ_{jM} and is hence on the left-hand side as the last expression. These aforementioned terms are not present for the first two time steps, however, because there are no convolution terms at the first time step, and the time derivative for ϕ used in the convolution at the second time step is known to be zero by virtue of the initial conditions. Thus, the left-hand side matrix has one set of coefficients for the first two time steps and another set of coefficients for each time step thereafter. The need for only two factorizations significantly reduces the computational effort necessary to solve the problem. Also advantageous is the fact that the current value of the unknown potential does not appear in the discretized convolution terms since $\frac{\partial G(f)}{\partial t} = = 0$ at $t = 0$ for all $\vec{x}$ [5].

We can see from (3.3) that, even with the aforementioned properties, computational burden will be high when the number of panels describing the body is high. The same is true with a large number of time steps. Thus, any means of shrinking the size of the system while maintaining desired accuracy would be favorable. A significant

reduction in problem size can be accomplished by exploiting body symmetry whenever possible. Most ships are symmetric about their longitudinal centerline. Hence, it is only necessary to discretize half the body which in turn reduces the number of unknowns by a factor of two.

The main computational burden in the solution of the linear system of equations comes from the calculation of the Green function coefficients. In all but the coarsest discretizations the number of Green function coefficients is quite large ($NP^2 \times M$) and so it is generally impractical to store these values in memory. This being the case, we have the option of either recalculating all the coefficients at each time step or calculating them once and storing them on disk where they are fetched when needed. On most workstations recalculating takes an average of five times longer so the store and fetch method is normally preferred unless disk space is scarce. This may change, however, as CPU speeds increase. Either way, we can approximate the necessary storage space (RAM or disk) as

$$\text{Storage} \propto NP^2M.$$

Likewise, we can approximate computational cost as [2]

$$\text{Cost} \propto NP^2M^2.$$

3.3 Determination of the Incident Potential

The determination of terms in (2.36) which relate to the body boundary condition as well as those necessary to calculate the Froude-Krylov force requires that we choose a representation of the velocity potential for the incident wave field. Because we wish to consider an excitation which contains all possible frequencies, we must choose an incident potential that is impulsive in nature for a chosen point (x, y) on the linearized free-surface. Given this stipulation, we may choose the incident potential of the form

shown in (2.79) and rewritten here

$$\phi^I(\vec{x},t) = \frac{1}{\pi}\Re\Big\{\int_0^\infty d\omega_e \frac{ig}{\omega} e^{[kz - ik(x\cos\beta + y\sin\beta) + i\omega_e t]}\Big\}, \tag{3.4}$$

where the wave number k is a function of absolute frequency such that $k(\omega) = \frac{\omega^2}{g}$, β is the angle of wave propagation, and the reference frame for the potential is the ship-fixed coordinate system.

Using the particular choice of incident potential detailed above, we may obtain expressions for the potential's spatial and time derivatives. In the case of head seas, we find

$$\vec{\nabla}\phi^I(\vec{x},t) = \frac{1}{\pi}\Re\Big\{\begin{bmatrix} \hat{i}\cos\beta \\ \hat{j}\sin\beta \\ \hat{k}i \end{bmatrix} \int_0^\infty d\omega(\omega - \frac{2\omega^2 U\cos\beta}{g}) \cdot$$

$$e^{\frac{\omega^2}{g}[z - i(x\cos\beta + y\sin\beta + Ut\cos\beta)]} e^{i\omega t}\Big\} \tag{3.5}$$

$$\phi_t^I(\vec{x},t) = -\frac{g}{\pi}\Re\Big\{\int_0^\infty d\omega(1 - \frac{3\omega U\cos\beta}{g} + \frac{2\omega^2 U^2\cos^2\beta}{g^2}) \cdot$$

$$e^{\frac{\omega^2}{g}[z - i(x\cos\beta + y\sin\beta + Ut\cos\beta)]} e^{i\omega t}\Big\}. \tag{3.6}$$

Likewise, in following seas we find

$$\vec{\nabla}\phi_1^I(\vec{x},t) = \frac{1}{\pi}\Re\Big\{\begin{bmatrix} \hat{i}\cos\beta \\ \hat{j}\sin\beta \\ \hat{k}i \end{bmatrix} \int_0^{\frac{g}{2U\cos\beta}} d\omega(\omega - \frac{2\omega^2 U\cos\beta}{g}) \cdot$$

$$e^{\frac{\omega^2}{g}[z-i(x\cos\beta+y\sin\beta+Ut\cos\beta)]}e^{i\omega t}\Big\} \tag{3.7}$$

$$\vec{\nabla}\phi_2^I(\vec{x},t)=\frac{1}{\pi}\Re\Big\{\begin{bmatrix}\hat{i}\cos\beta\\ \hat{j}\sin\beta\\ \hat{k}i\end{bmatrix}\int_{\frac{g}{2U\cos\beta}}^{\frac{g}{U\cos\beta}}d\omega(\omega-\frac{2\omega^2U\cos\beta}{g})\cdot$$

$$e^{\frac{\omega^2}{g}[z-i(x\cos\beta+y\sin\beta+Ut\cos\beta)]}e^{i\omega t}\Big\} \tag{3.8}$$

$$\vec{\nabla}\phi_3^I(\vec{x},t)=\frac{1}{\pi}\Re\Big\{\begin{bmatrix}\hat{i}\cos\beta\\ \hat{j}\sin\beta\\ \hat{k}i\end{bmatrix}\int_{\frac{g}{U\cos\beta}}^{\infty}d\omega(\omega-\frac{2\omega^2U\cos\beta}{g})\cdot$$

$$e^{\frac{\omega^2}{g}[z-i(x\cos\beta+y\sin\beta+Ut\cos\beta)]}e^{i\omega t}\Big\}$$

$$\phi_{1t}^I(\vec{x},t)=-\frac{g}{\pi}\Re\Big\{\int_0^{\frac{g}{2U\cos\beta}}d\omega(1-\frac{3\omega U\cos\beta}{g}+\frac{2\omega^2U^2\cos^2\beta}{g^2})\cdot$$

$$e^{\frac{\omega^2}{g}[z-i(x\cos\beta+y\sin\beta+Ut\cos\beta)]}e^{i\omega t}\Big\} \tag{3.9}$$

$$\phi_{2t}^I(\vec{x},t)=-\frac{g}{\pi}\Re\Big\{\int_{\frac{g}{2U\cos\beta}}^{\frac{g}{U\cos\beta}}d\omega(1-\frac{3\omega U\cos\beta}{g}+\frac{2\omega^2U^2\cos^2\beta}{g^2})\cdot$$

$$e^{\frac{\omega^2}{g}[z-i(x\cos\beta+y\sin\beta+Ut\cos\beta)]}e^{i\omega t}\Big\} \tag{3.10}$$

$$\phi^I_{3t}(\vec{x},t) = -\frac{g}{\pi}\Re\Big\{\int_{\frac{g}{U\cos\beta}}^{\infty} d\omega(1 - \frac{3\omega U\cos\beta}{g} + \frac{2\omega^2U^2\cos^2\beta}{g^2})\cdot$$

$$e^{\frac{\omega^2}{g}[z-i(x\cos\beta+y\sin\beta+Ut\cos\beta)]}e^{i\omega t}\Big\}, \qquad (3.11)$$

where the subscripts 1, 2, and 3 denote the specific absolute frequency ranges over which the integrals are taken. For the above expressions we have used (2.84) and (2.83) to obtain integrands which are a function of absolute frequency only. It is possible, therefore, to express all of these integrals in the form described in [11]:

$$I^{(n)}(\alpha,b) = \int x^n e^{-(\alpha x^2+2bx)}dx \qquad (3.12)$$

where

$$\begin{aligned} x &\longleftrightarrow \omega \\ \alpha &\longleftrightarrow \frac{1}{g}[-z + i(x\cos\beta + y\sin\beta + Ut\cos\beta)] \\ b &\longleftrightarrow -\frac{it}{2}. \end{aligned} \qquad (3.13)$$

We are interested in finding numerical solutions for the expressions $I^{(0)}(\alpha,b)$, $I^{(1)}(\alpha,b)$, and $I^{(2)}(\alpha,b)$ as they apply to both head and following seas cases. A solution for integrals of this type is given in [1] by equation (7.4.32) such that

$$\int e^{-(\alpha x^2+2bx+c)}dx = \frac{1}{2}\sqrt{\frac{\pi}{\alpha}}e^{\frac{b^2-\alpha c}{\alpha}}\mathrm{erf}(\sqrt{\alpha}x + \frac{b}{\sqrt{\alpha}}) + \text{Constant} \qquad (3.14)$$

where $\alpha \neq 0$ and erf is the error function. If we take $c = 0$, then by analogy we may conclude that in general

$$I^{(0)}(\alpha,b) = \int e^{-(\alpha x^2+2bx)}dx$$
$$= \frac{1}{2}\sqrt{\frac{\pi}{\alpha}}e^{\frac{b^2}{\alpha}}\mathrm{erf}(\sqrt{\alpha}x + \frac{b}{\sqrt{\alpha}}) + \text{Constant}. \tag{3.15}$$

Hence, it follows that by taking partial derivatives of (3.15) with respect to α and b, noting equation (7.1.19) in [1] which states

$$\frac{d^{n+1}}{dz^{n+1}}\mathrm{erf}(z) = (-1)^n\frac{2}{\sqrt{\pi}}H_n(z)e^{-z^2} \tag{3.16}$$

where

$H_n \equiv$ Hermite polynomial of order n

$H_0 = 1,$

we may likewise determine $I^{(1)}(\alpha,b)$ and $I^{(2)}(\alpha,b)$ in terms of error functions. Beginning with $I^{(1)}(\alpha,b)$, we find

$$\frac{\partial}{\partial b}\int e^{-(\alpha x^2+2bx)}dx = -2\int xe^{-(\alpha x^2+2bx)}dx \tag{3.17}$$

and so

$$I^{(1)}(\alpha,b) = \int xe^{-(\alpha x^2+2bx)}dx = \frac{\partial}{\partial b}\Big(-\frac{1}{4}\sqrt{\frac{\pi}{\alpha}}e^{\frac{b^2}{\alpha}}\mathrm{erf}(\sqrt{\alpha}x + \frac{b}{\sqrt{\alpha}})\Big)$$
$$= -\frac{b}{2\alpha}\sqrt{\frac{\pi}{\alpha}}e^{\frac{b^2}{\alpha}}\mathrm{erf}(\sqrt{\alpha}x + \frac{b}{\sqrt{\alpha}}) - \frac{1}{2\alpha}e^{\frac{b^2}{\alpha}}e^{-(\alpha x^2+2bx+\frac{b^2}{\alpha})}. \tag{3.18}$$

Similarly, for $I^{(2)}(\alpha,b)$ we find

$$\frac{\partial}{\partial\alpha}\int e^{-(\alpha x^2+2bx)}dx = -\int x^2 e^{-(\alpha x^2+2bx)}dx \tag{3.19}$$

and so

$$I^{(2)}(\alpha,b) = \int x^2 e^{-(\alpha x^2+2bx)}dx = \frac{\partial}{\partial\alpha}\Big(-\frac{1}{2}\sqrt{\frac{\pi}{\alpha}}e^{\frac{b^2}{\alpha}}\mathrm{erf}(\sqrt{\alpha}x+\frac{b}{\sqrt{\alpha}})\Big)$$

$$= \frac{1}{4\alpha}\sqrt{\frac{\pi}{\alpha}}e^{\frac{b^2}{\alpha}}\mathrm{erf}(\sqrt{\alpha}x+\frac{b}{\sqrt{\alpha}}) + \frac{b^2}{2\alpha^2}\sqrt{\frac{\pi}{\alpha}}e^{\frac{b^2}{\alpha}}\mathrm{erf}(\sqrt{\alpha}x+\frac{b}{\sqrt{\alpha}})$$

$$-\frac{1}{2}e^{\frac{b^2}{\alpha}}(\frac{x}{\alpha}-\frac{b}{\alpha^2})e^{-(\alpha x^2+2bx+\frac{b^2}{\alpha})}. \tag{3.20}$$

We may now extend these general expressions to cover the specific cases of head seas and following seas. For head seas, we wish to evaluate the integrals over the interval $[0,\infty]$. Noting from equation (7.1.16) in [1] that

$$\mathrm{erf}(z) \to 1 \qquad \text{as } z \to \infty \text{ in } |\arg z| < \frac{\pi}{4},$$

and following the procedure used in [11], we obtain the expressions

$$I^{(0)}(\alpha,b) = \frac{1}{2}\sqrt{\frac{\pi}{\alpha}}e^{\frac{b^2}{\alpha}}[1-\mathrm{erf}(\frac{b}{\sqrt{\alpha}})] \tag{3.21}$$

$$I^{(1)}(\alpha,b) = -\frac{b}{2\alpha}\sqrt{\frac{\pi}{\alpha}}e^{\frac{b^2}{\alpha}}[1-\mathrm{erf}(\frac{b}{\sqrt{\alpha}})] + \frac{1}{2\alpha} \tag{3.22}$$

$$I^{(2)}(\alpha,b) = (\frac{1}{4\alpha} - \frac{b^2}{2\alpha^2}\sqrt{\frac{\pi}{\alpha}}e^{\frac{b^2}{\alpha}}[1 - \text{erf}(\frac{b}{\sqrt{\alpha}})] - \frac{b}{2\alpha^2}. \tag{3.23}$$

We now relate the error function, erf(z), with the complimentary error function, erfc(z), using equation (7.1.2) from [1]

$$\text{erfc}(z) = 1 - \text{erf}(z) \tag{3.24}$$

and so we can determine the integrals of interest written recursively

$$I^{(0)}(\alpha,b) = \frac{1}{2}\sqrt{\frac{\pi}{\alpha}}e^{\frac{b^2}{\alpha}}\text{erfc}(\frac{b}{\sqrt{\alpha}}) \tag{3.25}$$

$$I^{(1)}(\alpha,b) = -\frac{b}{\alpha}I_0(\alpha,b) + \frac{1}{2\alpha} \tag{3.26}$$

$$I^{(2)}(\alpha,b) = \frac{1}{2\alpha}I_0(\alpha,b) - \frac{b}{\alpha}I_1(\alpha,b). \tag{3.27}$$

Finally, for implementation in the numerical scheme, we wish to calculate (3.25), (3.26), and (3.27) in a robust manner. In order to do so, we use the relation found in equation (7.1.3) of [1]

$$\text{w}(z) = e^{-z^2}\text{erfc}(-iz) \tag{3.28}$$

which gives

$$I^{(0)}(\alpha, b) = \frac{1}{2}\sqrt{\frac{\pi}{\alpha}}\mathrm{w}(\frac{ib}{\sqrt{\alpha}}) \tag{3.29}$$

and is calculated using the algorithm developed by Gautschi [7].

In the case of following seas, we may determine the integral quantities in a similar fashion; however, we now must evaluate the integrals individually over the three specific ranges of absolute frequency. Denoting these ranges with subscripts we find:

$$I_1^{(0)}(\alpha, b) = \int_0^{\frac{g}{2U\cos\beta}} \mathrm{e}^{-(\alpha x^2 + 2bx)} dx$$

$$= \frac{1}{2}\sqrt{\frac{\pi}{\alpha}}\mathrm{e}^{\frac{b^2}{\alpha}}[\mathrm{erf}(\frac{g\sqrt{\alpha}}{2U\cos\beta} + \frac{b}{\sqrt{\alpha}}) - \mathrm{erf}(\frac{b}{\sqrt{\alpha}})] \tag{3.30}$$

$$I_2^{(0)}(\alpha, b) = \int_{\frac{g}{2U\cos\beta}}^{\frac{g}{U\cos\beta}} \mathrm{e}^{-(\alpha x^2 + 2bx)} dx$$

$$= \frac{1}{2}\sqrt{\frac{\pi}{\alpha}}\mathrm{e}^{\frac{b^2}{\alpha}}[\mathrm{erf}(\frac{g\sqrt{\alpha}}{U\cos\beta} + \frac{b}{\sqrt{\alpha}}) - \mathrm{erf}(\frac{g\sqrt{\alpha}}{2U\cos\beta} + \frac{b}{\sqrt{\alpha}})] \tag{3.31}$$

$$I_3^{(0)}(\alpha, b) = \int_{\frac{g}{U\cos\beta}}^{\infty} \mathrm{e}^{-(\alpha x^2 + 2bx)} dx$$

$$= \frac{1}{2}\sqrt{\frac{\pi}{\alpha}}\mathrm{e}^{\frac{b^2}{\alpha}}[1 - \mathrm{erf}(\frac{g\sqrt{\alpha}}{U\cos\beta} + \frac{b}{\sqrt{\alpha}})]. \tag{3.32}$$

Similarly

$$I_1^{(1)}(\alpha, b) = \frac{1}{2}\sqrt{\frac{\pi}{\alpha}}\mathrm{e}^{\frac{b^2}{\alpha}}[\mathrm{erf}(\frac{g\sqrt{\alpha}}{2U\cos\beta} + \frac{b}{\sqrt{\alpha}}) - \mathrm{erf}(\frac{b}{\sqrt{\alpha}})]$$

$$-\frac{1}{2\alpha}e^{\frac{b^2}{\alpha}}[e^{-(\frac{g^2\alpha}{4U^2\cos^2\beta}+\frac{gb}{U\cos\beta}+\frac{b^2}{\alpha})}-e^{-\frac{b^2}{\alpha}}]$$

$$=-\frac{b}{\alpha}I_1^{(0)}(\alpha,b)-\frac{1}{2\alpha}e^{-(\frac{g^2\alpha}{4U^2\cos^2\beta}+\frac{gb}{U\cos\beta})}+\frac{1}{2\alpha} \tag{3.33}$$

$$I_2^{(1)}(\alpha,b)=-\frac{b}{2\alpha}\sqrt{\frac{\pi}{\alpha}}e^{\frac{b^2}{\alpha}}[\mathrm{erf}(\frac{g\sqrt{\alpha}}{U\cos\beta}+\frac{b}{\sqrt{\alpha}})-\mathrm{erf}(\frac{g\sqrt{\alpha}}{2U\cos\beta}+\frac{b}{\sqrt{\alpha}})]$$
$$-\frac{1}{2\alpha}e^{\frac{b^2}{\alpha}}[e^{-(\frac{g^2\alpha}{U^2\cos^2\beta}+\frac{2gb}{U\cos\beta}+\frac{b^2}{\alpha})}-e^{-(\frac{g^2\alpha}{4U^2\cos^2\beta}+\frac{gb}{U\cos\beta}+\frac{b^2}{\alpha})}]$$

$$=-\frac{b}{\alpha}I_2^{(0)}(\alpha,b)-\frac{1}{2\alpha}[e^{-(\frac{g^2\alpha}{U^2\cos^2\beta}+\frac{2gb}{U\cos\beta})}-e^{-(\frac{g^2\alpha}{4U^2\cos^2\beta}+\frac{gb}{U\cos\beta})}] \tag{3.34}$$

$$I_3^{(1)}(\alpha,b)=-\frac{b}{2\alpha}\sqrt{\frac{\pi}{\alpha}}e^{\frac{b^2}{\alpha}}[1-\mathrm{erf}(\frac{g\sqrt{\alpha}}{U\cos\beta}+\frac{b}{\sqrt{\alpha}})]$$
$$+\frac{1}{2\alpha}e^{\frac{b^2}{\alpha}}e^{-(\frac{g^2\alpha}{U^2\cos^2\beta}+\frac{2gb}{U\cos\beta}+\frac{b^2}{\alpha})}$$

$$=-\frac{b}{\alpha}I_3^{(0)}(\alpha,b)+\frac{1}{2\alpha}e^{-(\frac{g^2\alpha}{U^2\cos^2\beta}+\frac{2gb}{U\cos\beta})} \tag{3.35}$$

and

$$I_1^{(2)}(\alpha,b)=\frac{1}{4\alpha}\sqrt{\frac{\pi}{\alpha}}e^{\frac{b^2}{\alpha}}[\mathrm{erf}(\frac{g\sqrt{\alpha}}{2U\cos\beta}+\frac{b}{\sqrt{\alpha}})-\mathrm{erf}(\frac{b}{\sqrt{\alpha}})]$$
$$+\frac{b^2}{2\alpha^2}\sqrt{\frac{\pi}{\alpha}}e^{\frac{b^2}{\alpha}}[\mathrm{erf}(\frac{g\sqrt{\alpha}}{2U\cos\beta}+\frac{b}{\sqrt{\alpha}})-\mathrm{erf}(\frac{b}{\sqrt{\alpha}})]$$
$$-\frac{1}{2}e^{\frac{b^2}{\alpha}}(\frac{g}{2\alpha U\cos\beta}-\frac{b}{\alpha^2})e^{-(\frac{g^2\alpha}{4U^2\cos^2\beta}+\frac{gb}{U\cos\beta}+\frac{b^2}{\alpha})}$$
$$-\frac{b}{2\alpha^2}e^{\frac{b^2}{\alpha}}e^{-\frac{b^2}{\alpha}}$$

$$=\frac{1}{2\alpha}I_1^{(0)}(\alpha,b)-\frac{b}{\alpha}I_1^{(1)}(\alpha,b)-\frac{g}{4\alpha U\cos\beta}e^{-(\frac{g^2\alpha}{4U^2\cos^2\beta}+\frac{gb}{U\cos\beta})} \tag{3.36}$$

$$I_2^{(2)}(\alpha,b) = \frac{1}{4\alpha}\sqrt{\frac{\pi}{\alpha}}e^{\frac{b^2}{\alpha}}[\mathrm{erf}(\frac{g\sqrt{\alpha}}{U\cos\beta}+\frac{b}{\sqrt{\alpha}}) - \mathrm{erf}(\frac{g\sqrt{\alpha}}{2U\cos\beta}+\frac{b}{\sqrt{\alpha}})]$$
$$\frac{b^2}{2\alpha^2}\sqrt{\frac{\pi}{\alpha}}e^{\frac{b^2}{\alpha}}[\mathrm{erf}(\frac{g\sqrt{\alpha}}{U\cos\beta}+\frac{b}{\sqrt{\alpha}}) - \mathrm{erf}(\frac{g\sqrt{\alpha}}{2U\cos\beta}+\frac{b}{\sqrt{\alpha}})]$$
$$-\frac{1}{2}e^{\frac{b^2}{\alpha}}(\frac{g}{\alpha U\cos\beta}-\frac{b}{\alpha^2})e^{-(\frac{g^2\alpha}{U^2\cos^2\beta}+\frac{2gb}{U\cos\beta}+\frac{b^2}{\alpha})}$$
$$+\frac{1}{2}e^{\frac{b^2}{\alpha}}(\frac{g}{2\alpha U\cos\beta}-\frac{b}{\alpha^2})e^{-(\frac{g^2\alpha}{4U^2\cos^2\beta}+\frac{gb}{U\cos\beta}+\frac{b^2}{\alpha})}]$$

$$= \frac{1}{2\alpha}I_2^{(0)}(\alpha,b) - \frac{b}{\alpha}I_2^{(1)}(\alpha,b) - \frac{g}{2\alpha U\cos\beta}e^{-(\frac{g^2\alpha}{U^2\cos^2\beta}+\frac{2gb}{U\cos\beta})}$$
$$+\frac{g}{4\alpha U\cos\beta}e^{-(\frac{g^2\alpha}{4U^2\cos^2\beta}+\frac{gb}{U\cos\beta})} \qquad (3.37)$$

$$I_3^{(2)}(\alpha,b) = \frac{1}{4\alpha}\sqrt{\frac{\pi}{\alpha}}e^{\frac{b^2}{\alpha}}[1-\mathrm{erf}(\frac{g\sqrt{\alpha}}{U\cos\beta}+\frac{b}{\sqrt{\alpha}})]$$
$$+\frac{b^2}{2\alpha^2}\sqrt{\frac{\pi}{\alpha}}e^{\frac{b^2}{\alpha}}[1-\mathrm{erf}(\frac{g\sqrt{\alpha}}{U\cos\beta}+\frac{b}{\sqrt{\alpha}})]$$
$$+\frac{1}{2}e^{\frac{b^2}{\alpha}}(\frac{g}{\alpha U\cos\beta}-\frac{b}{\alpha^2})e^{-(\frac{g^2\alpha}{U^2\cos^2\beta}+\frac{2gb}{U\cos\beta}+\frac{b^2}{\alpha})}$$

$$= \frac{1}{2\alpha}I_3^{(0)}(\alpha,b) - \frac{b}{\alpha}I_3^{(1)}(\alpha,b) + \frac{g}{2\alpha U\cos\beta}e^{-(\frac{g^2\alpha}{U^2\cos^2\beta}+\frac{2gb}{U\cos\beta})}. \qquad (3.38)$$

Again using (3.24) we can write

$$I_1^{(0)}(\alpha,b) = \frac{1}{2}\sqrt{\frac{\pi}{\alpha}}e^{\frac{b^2}{\alpha}}[\mathrm{erfc}(\frac{b}{\sqrt{\alpha}} - \mathrm{erfc}(\frac{g\sqrt{\alpha}}{2U\cos\beta}+\frac{b}{\sqrt{\alpha}})] \qquad (3.39)$$

$$I_2^{(0)}(\alpha,b) = \frac{1}{2}\sqrt{\frac{\pi}{\alpha}}e^{\frac{b^2}{\alpha}}[\mathrm{erfc}(\frac{g\sqrt{\alpha}}{2U\cos\beta}+\frac{b}{\sqrt{\alpha}}) - \mathrm{erfc}(\frac{g\sqrt{\alpha}}{U\cos\beta}+\frac{b}{\sqrt{\alpha}})] \qquad (3.40)$$

$$I_3^{(0)}(\alpha,b)=\frac{1}{2}\sqrt{\frac{\pi}{\alpha}}\mathrm{e}^{\frac{b^2}{\alpha}}[\mathrm{erfc}(\frac{g\sqrt{\alpha}}{U\cos\beta}+\frac{b}{\sqrt{\alpha}})], \tag{3.41}$$

and using (3.28) we can rewrite all of the integrals in terms of $w(z)$ as

$$I_1^{(0)}(\alpha,b)=\frac{1}{2}\sqrt{\frac{\pi}{\alpha}}[\mathrm{w}(\frac{ib}{\sqrt{\alpha}})-\mathrm{e}^{-(\frac{g^2\alpha}{4U^2\cos^2\beta}+gbU\cos\beta)}\mathrm{w}(\frac{ig\sqrt{\alpha}}{2U\cos\beta}+\frac{ib}{\sqrt{\alpha}})] \tag{3.42}$$

$$\begin{aligned}I_2^{(0)}(\alpha,b)=\frac{1}{2}\sqrt{\frac{\pi}{\alpha}}[&\mathrm{e}^{-(\frac{g^2\alpha}{4U^2\cos^2\beta}+gbU\cos\beta)}\mathrm{w}(\frac{ig\sqrt{\alpha}}{2U\cos\beta}+\frac{ib}{\sqrt{\alpha}})\\&-\mathrm{e}^{-(\frac{g^2\alpha}{U^2\cos^2\beta}+2gbU\cos\beta)}\mathrm{w}(\frac{ig\sqrt{\alpha}}{U\cos\beta}+\frac{ib}{\sqrt{\alpha}})]\end{aligned} \tag{3.43}$$

$$I_3^{(0)}(\alpha,b)=\frac{1}{2}\sqrt{\frac{\pi}{\alpha}}[\mathrm{e}^{-(\frac{g^2\alpha}{U^2\cos^2\beta}+2gbU\cos\beta)}\mathrm{w}(\frac{ig\sqrt{\alpha}}{U\cos\beta}+\frac{ib}{\sqrt{\alpha}})]. \tag{3.44}$$

Finally, we can find the potential expressions detailed in (3.5) through (3.11) using the numerically obtainable integrals $I^{(n)}(\alpha,b)$, i.e., for head seas

$$\vec{\nabla}\phi^I(\vec{x},t)=\frac{1}{\pi}\Re\Big\{\begin{bmatrix}\hat{i}\cos\beta\\ \hat{j}\sin\beta\\ \hat{k}i\end{bmatrix}\Big(I^{(1)}(\alpha,b)-\frac{2U\cos\beta}{g}I^{(2)}(\alpha,b)\Big)\Big\} \tag{3.45}$$

$$\begin{aligned}\phi_t^I(\vec{x},t)=-\frac{g}{\pi}\Re\Big\{\Big(&I^{(0)}(\alpha,b)-\frac{3U\cos\beta}{g}I^{(1)}(\alpha,b)\\&+\frac{2U^2\cos^2\beta}{g^2}I^{(2)}(\alpha,b)\Big)\Big\}\end{aligned} \tag{3.46}$$

and for following seas

$$\vec{\nabla}\phi_m^I(\vec{x},t) = \frac{1}{\pi}\Re\Big\{ \begin{bmatrix} \hat{i}\cos\beta \\ \hat{j}\sin\beta \\ \hat{k}i \end{bmatrix} \Big(I_m^{(1)}(\alpha,b) - \frac{2U\cos\beta}{g} I_m^{(2)}(\alpha,b)\Big)\Big\} \tag{3.47}$$

$$\phi_{mt}^I(\vec{x},t) = -\frac{g}{\pi}\Re\Big\{\Big(I_m^{(0)}(\alpha,b) - \frac{3U\cos\beta}{g} I_m^{(1)}(\alpha,b) + \frac{2U^2\cos^2\beta}{g^2} I_m^{(2)}(\alpha,b)\Big)\Big\} \tag{3.48}$$

for $m = 1, 2, 3$.

3.4 Calculation of the Wave Elevation

As mentioned earlier, we need to obtain the time dependent exciting force in order to perform simulations of ship motions. This is accomplished by convolving the ship's impulse-response function for the required mode of motion with input wave elevation information. Because we choose our incident potential to be in the ship-fixed frame of reference, we also must have the input wave elevation information in the ship-fixed frame. This necessity can pose a problem since it is most common to take wave elevation measurements from a fixed point. Therefore, we must transform this fixed point information into ship-fixed information. Theoretically, we have already discussed the transformation process in subsection (2.7). We now turn our attention to the problem of practical computation.

In the case of head seas, the numerical computation of wave elevation input in the ship-fixed frame is relatively straight-forward. Since there is no frequency ambiguity with head seas, we are left with the expression

$$\zeta(t) = \Re\{\frac{1}{\pi}\int_0^\infty d\omega_e \frac{\bar{\zeta}(\omega)}{1 - \frac{2U\omega\cos\beta}{g}} e^{i\omega_e t}\}. \tag{3.49}$$

We may then easily compute the wave elevation time history using a simple quadrature scheme such as Filon integration with no modifications to the equations.

The case of following seas is somewhat more complicated, however. We recall that ambiguity in encounter frequency dictates the need for wave elevation information in three distinct frequency ranges:

$$\zeta_1(t) = \Re\{\frac{1}{\pi}\int_0^{g/4U\cos\beta} d\omega_e \frac{\bar{\zeta}(\omega_1)}{1-\frac{2U\omega_1\cos\beta}{g}} e^{i\omega_e t}\} \tag{3.50}$$

$$\zeta_2(t) = \Re\{\frac{1}{\pi}\int_0^{g/4U\cos\beta} d\omega_e \frac{\bar{\zeta}(\omega_2)}{1-\frac{2U\omega_2\cos\beta}{g}} e^{i\omega_e t}\} \tag{3.51}$$

$$\zeta_3(t) = \Re\{\frac{1}{\pi}\int_0^{\infty} d\omega_e \frac{\bar{\zeta}(\omega_3)}{1-\frac{2U\omega_3\cos\beta}{g}} e^{i\omega_e t}\}. \tag{3.52}$$

We can see that equation (3.52) may be computed in a fashion similar to (3.49), but (3.50) and (3.51) pose a problem since their integrands become singular at the limit $\omega_e = g/4U\cos\beta$, a situation which becomes clear when we substitute equations (2.96) and (2.97) respectively. For convenience, we reprint these relations here:

$$\omega_1 = \frac{g}{2U\cos\beta}\left(1-\sqrt{1-\frac{4U\cos\beta}{g}\omega_e}\right) \tag{3.53}$$

$$\omega_2 = \frac{g}{2U\cos\beta}\left(1+\sqrt{1-\frac{4U\cos\beta}{g}\omega_e}\right) \tag{3.54}$$

There are, however, two methods we can use to overcome this difficulty which are outlined below.

In the first method, we derive expressions which contain only a square root singu-

larity and are thereby computable by standard numerical schemes. This transformation may be accomplished by rewriting the denominator of the integrand as a function of encounter frequency using the above relations (3.53) and (3.54). If we define

$$\omega_u \equiv \frac{g}{4U\cos\beta}$$

we can write

$$\zeta_1(t) = \Re\{\frac{-1}{\pi}\int_0^{\omega_u} d\omega_e \frac{\bar{\zeta}(\omega_1)}{\sqrt{1-\omega_e/\omega_u}} e^{i\omega_e t}\} \tag{3.55}$$

$$\zeta_2(t) = \Re\{\frac{1}{\pi}\int_0^{\omega_u} d\omega_e \frac{\bar{\zeta}(\omega_2)}{\sqrt{1-\omega_e/\omega_u}} e^{i\omega_e t}\}. \tag{3.56}$$

For reasons of computational efficiency, we would like to keep the range over which the integrand with the singular limit is evaluated as small as possible. To this effect, we can split the range of evaluation to create a regular piece and a singular piece. Using $\zeta_1(t)$ as an example, we find

$$\begin{aligned}\zeta_1(t) &= \zeta_1^{(R)}(t) + \zeta_1^{(S)}(t) \\ &= \Re\{\frac{-1}{\pi}\int_0^{\omega_i} d\omega_e \frac{\bar{\zeta}(\omega_1)}{\sqrt{1-\omega_e/\omega_u}} e^{i\omega_e t}\} \\ &+\Re\{\frac{-1}{\pi}\int_{\omega_i}^{\omega_u} d\omega_e \frac{\bar{\zeta}(\omega_1)}{\sqrt{1-\omega_e/\omega_u}} e^{i\omega_e t}\}\end{aligned} \tag{3.57}$$

where ω_i is a predefined intermediate value of encounter frequency. If we now look only at the singular part, we can deal with the square root singularity by using the

identity

$$\int_a^b f(\omega)d\omega = \int_0^{\sqrt{b-a}} 2\gamma f(b-\gamma^2)d\gamma \tag{3.58}$$

and so obtain the expression

$$\zeta_1^{(S)}(t) = \Re\{\frac{-2\sqrt{\omega_u}}{\pi}\int_0^{\sqrt{\omega_u-\omega_i}} d\gamma\bar{\zeta}(\omega_u-\gamma^2)e^{i(\omega_u-\gamma^2)t)}\}. \tag{3.59}$$

Therefore, we can compute $\zeta_1(t)$ using the expression

$$\zeta_1(t) = \Re\{\frac{-1}{\pi}\int_0^{\omega_i} d\omega_e \frac{\bar{\zeta}(\omega_1)}{\sqrt{1-\omega_e/\omega_u}}e^{i\omega_e t}\}$$

$$+\Re\{\frac{-2\sqrt{\omega_u}}{\pi}\int_0^{\sqrt{\omega_u-\omega_i}} d\gamma\bar{\zeta}(\omega_u-\gamma^2)e^{i(\omega_u-\gamma^2)t)}\}. \tag{3.60}$$

Likewise, we can find a similar expression for $\zeta_2(t)$:

$$\zeta_2(t) = \Re\{\frac{1}{\pi}\int_0^{\omega_i} d\omega_e \frac{\bar{\zeta}(\omega_2)}{\sqrt{1-\omega_e/\omega_u}}e^{i\omega_e t}\}$$

$$+\Re\{\frac{2\sqrt{\omega_u}}{\pi}\int_0^{\sqrt{\omega_u-\omega_i}} d\gamma\bar{\zeta}(\omega_u-\gamma^2)e^{i(\omega_u-\gamma^2)t)}\}. \tag{3.61}$$

The second and perhaps more intuitive method is to express the wave elevation integrals entirely in terms of absolute frequency. In so doing, we are able to remove the singularity completely and are able to obtain the wave elevation time history in the form

$$\zeta_1(t) = \Re\{\frac{1}{\pi}\int_0^{g/2U\cos\beta} d\omega_1\bar{\zeta}(\omega_1)e^{i\omega_1(1-\frac{\omega_1 U\cos\beta}{g})t)}\} \tag{3.62}$$

$$\zeta_2(t) = \Re\{\frac{1}{\pi}\int_{g/2U\cos\beta}^{g/U\cos\beta} d\omega_2 \bar{\zeta}(\omega_2) e^{i\omega_2(1-\frac{\omega_2 U\cos\beta}{g})t)}\} \tag{3.63}$$

$$\zeta_3(t) = \Re\{\frac{1}{\pi}\int_{g/U\cos\beta}^{\infty} d\omega_3 \bar{\zeta}(\omega_3) e^{i\omega_3(1-\frac{\omega_3 U\cos\beta}{g})t)}\}. \tag{3.64}$$

3.5 Simulation

One goal of determining the various hydrodynamic and hydrostatic quantities involved in the ship motions problem is the ability to analyze seakeeping characteristics through the use of simulation. In this process, we may determine the ship's movements as it steadily translates through a prescribed incident wave field. In order to perform the simulation, we must integrate the equations of motion for the ship in time. In obtaining the equations of motion we again assume rigid-body motion with six degrees of freedom considering small perturbations about the mean body position. Given a linear system, we may then write the equations of motion in a similar fashion to that found in Cummins [3]

$$\sum_{k=1}^{6}[(M_{jk}+\mu_{jk})\ddot{x}_k(t) + b_{jk}\dot{x}_k(t) + (C_{jk}+c_{jk})x_k(t)$$

$$+\int_{-\infty}^{t} d\tau K_{jk}(t-\tau)x_k(\tau)] = X_j(t) \qquad j = 1,2,\cdots,6, \tag{3.65}$$

where

$$X_j(t) = \int_{-\infty}^{\infty} d\tau K_{jD}(t-\tau)\zeta(\tau)$$

In this equation, M_{jk} constitutes the ship's mass moment of inertia matrix, C_{jk} is the

matrix of hydrostatic restoring force coefficients, μ_{jk}, b_{jk}, and c_{jk} are hydrodynamic coefficients obtained from solution of the radiation problem, and $X_j(t)$ represents the time dependent exciting forces. The convolution integral on the left-hand side of the equation, whose kernel is a product of radiation impulse-response fuctions $K_{jk}(t)$ and displacement $x_k(t)$, is a consequence of the ship's radiated waves which, when generated, affect the ship at each successive time step. Likewise, the right-hand side exciting forces are represented by a similar convolution. The upper integration limit of ∞ in this convolution can be attributed to the dispersive nature of the incident wave system. We have defined the incident wave field impulsively such that it includes waves of all frequencies which coalesce at time $t = 0$. Hence, some disturbance is experienced before $t = 0$ due to the dispersed waves and requires that the impulse-response function has value at times less than zero. It should be noted that this representation of the equations of motion differs from that given by Cummins [3] only in that the convolution for the memory function is taken with displacement as opposed to velocity.

From numerical integration of (3.65) we may obtain time-domain histories of ship responses in the six degrees of freedom. These time histories may be validated if we compute frequency-domain response amplitude operators (RAOs) from the input and output signals:

$$RAO_j = \frac{|X_j(\omega)|}{|\zeta(\omega)|}. \tag{3.66}$$

$X_j(\omega)$ and $\zeta(\omega)$ are determined by taking the Fourier transforms of the output and input signals respectively.

Chapter 4

Numerical Results

The numerical scheme discussed in chapter 3 has been incorporated into the suite of programs called T$\bar{\text{I}}$MIT . As well as solving for the exciting force impulse-response functions for the six rigid-body modes of motion, these programs evaluate the time histories of the canonical potential values on each panel for both the radiation and diffraction problems, determine the hydrostatic and hydrodynamic coefficients, and solve for the radiation problem impulse-response funtions [5]. All input and output quantities are suitably non-dimensionalized as explained below:

$$\text{Ship Speed: } U^* = \frac{U}{\sqrt{gL}}$$

$$\text{Spatial Dimensions: } \vec{x}^* = \frac{\vec{x}}{L}$$

$$\text{Time: } t^* = \frac{t}{\sqrt{g/L}}$$

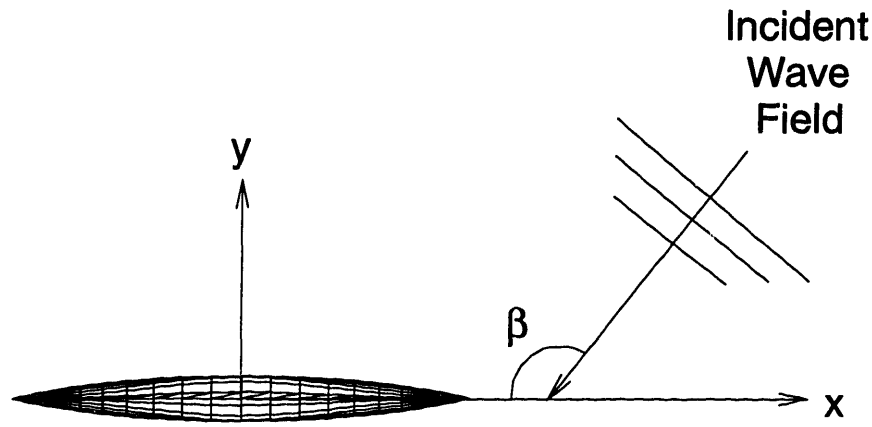

Figure 4-1: Definition for the incident wave angle heading.

$$\text{Impulse-response Function: } K^*_{jD} = \frac{K_{jD}}{\rho \zeta_a L^k g / L}$$

$$k = 3 \text{ for } j = 1, 2, 3$$

$$k = 4 \text{ for } j = 4, 5, 6.$$

Hereafter, the stars will be dropped and the non-dimensionalized form implied unless otherwise stated. A graphical representation for the definition of the wave heading angle may be found in Figure (4-1). This definition means that for head seas $\beta = \pi$ and for following seas $\beta = 0$. Straight beam seas are given when $\beta = \pm\frac{\pi}{2}$.

All numerical results presented here were obtained using an IRIS Indigo workstation. Both spatial and temporal discretizations were as coarse as possible while maintaining converged results. The numerical experiments were run using a Wigley

hullform with non-dimensional characteristics as follows:

$$\text{Length} = 1.0$$

$$\text{Beam} = 0.1$$

$$\text{Draft} = 0.0625$$

$$\text{Midship Section Coefficient} = 0.909.$$

This hullform corresponds to Wigley model 1 which was used to obtain experimental data by Journée [10].

4.1 Zero Speed Results

Zero speed calculations are merely a special case of the forward speed model presented in section 2.3. A quick review of equation (2.36) shows that the waterline integral vanishes for $U = 0$ and so there are no waterine effects. The zero speed results are interesting in as much as they are readily verifiable. There are some experimental data available as well as a number of reliable computer programs which solve the zero speed seakeeping problem in the frequency domain. Hence, comparison with existing results provides a good initial verification for the numerical model.

Figure (4-2) shows three snapshots in time of the typical incident wave profile encountered by the stationary vessel - one before the waves have coalesced, one at the point of coalescence, and one after the waves have begun to disperse. As is pointed out in [2], these profiles have actually had a small amount of the short wavelength contribution filtered out since we are evaluating

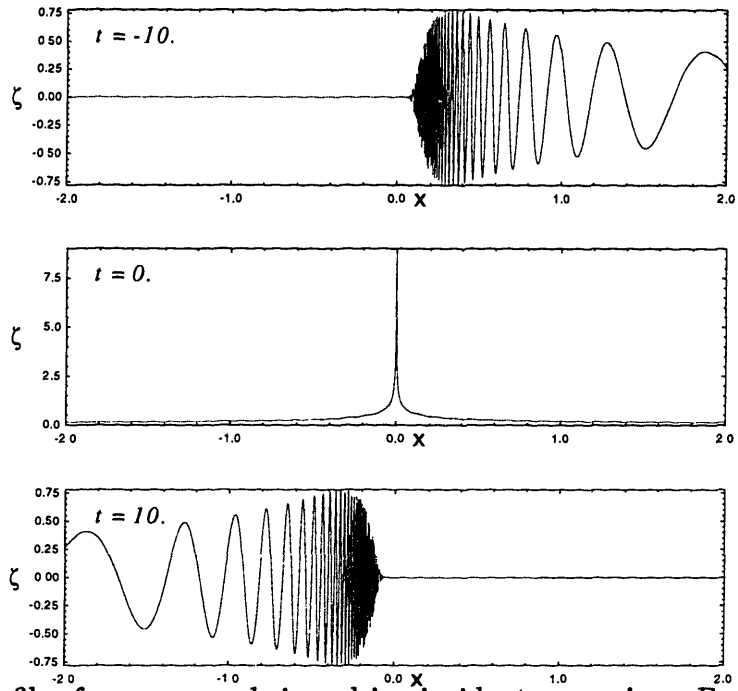

Figure 4-2: Profiles for an example impulsive incident wave given $F_n = 0.0$ and $\beta = \pi$ [2].

$$\zeta(\vec{x},t) \cong -\frac{1}{g}\phi_t^I(x,y,-0.001,t)$$

and the waves are attenuated exponentially as we move away from the free surface. Because we evaluate the potentials at the panel centroids, the filtering of short waves is present in the results. This effect is not entirely detrimental, however. The fact that we approximate the body by plane panels and the potentials by piecewise constants means that we are unable to resolve wavelengths which are not substantially longer than the panel dimensions. The presence of very short wavelengths can then cause numerical errors, although they are irrelevant in most cases. Hence, the filtering can help remove these anomolies.

Impulse-response functions for the heave exciting forces and pitch exciting moments of a stationary Wigley hull in head seas are shown in Figures (4-3) and (4-4) respectively. Because the Wigley hull form is a nice shape that provides no computational difficulties (i.e., it is wall-sided, has no flair, etc.), relatively few panels are

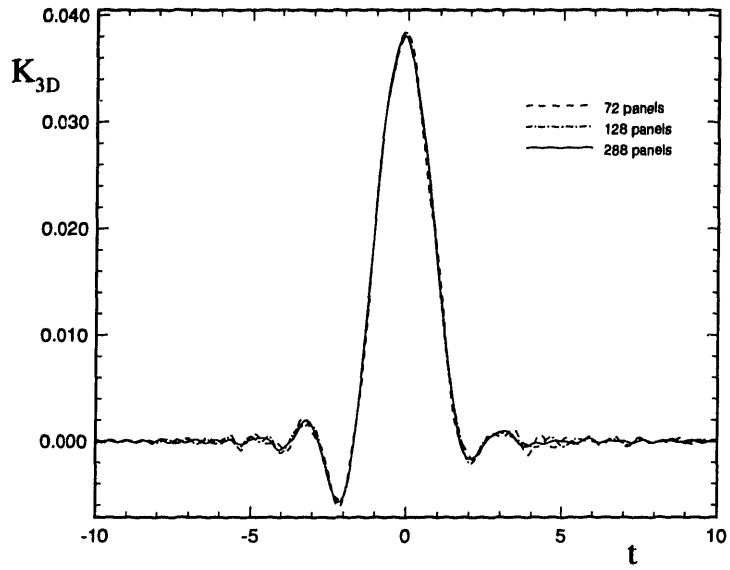

Figure 4-3: Heave exciting force impulse-response function for a Wigley hull travelling at $F_n = 0.0$ in head seas.

needed to obtain converged results. In this case, converged results were obtained with a panelization of 144 panels over the half-body exploiting port/starboard symmetry.

For verification purposes, these results were converted to the frequency domain by the Fourier transform

$$X_j(\omega) = \int_{-\infty}^{\infty} dt K_{jD}(t) \mathrm{e}^{-i\omega t} \tag{4.1}$$

where the transform has been numerically calculated using Filon quadrature based on equations (25.4.47) through (25.4.56) in [1]. For this quadrature scheme, a time step corresponding to converged impulse-response function results is used ($\Delta t = 0.1$) and equations (25.4.47) and (25.4.54) have been truncated to exclude terms of order Δt^5 and higher. Figure (4-5) shows the magnitude of the frequency dependent heave exciting force and likewise Figure (4-6) shows the magnitude of the frequency dependent pitch exciting moment. Both sets of results are compared with similar quantities calculated by WAMIT, a frequency domain analog of T[I]MIT [4]. We can

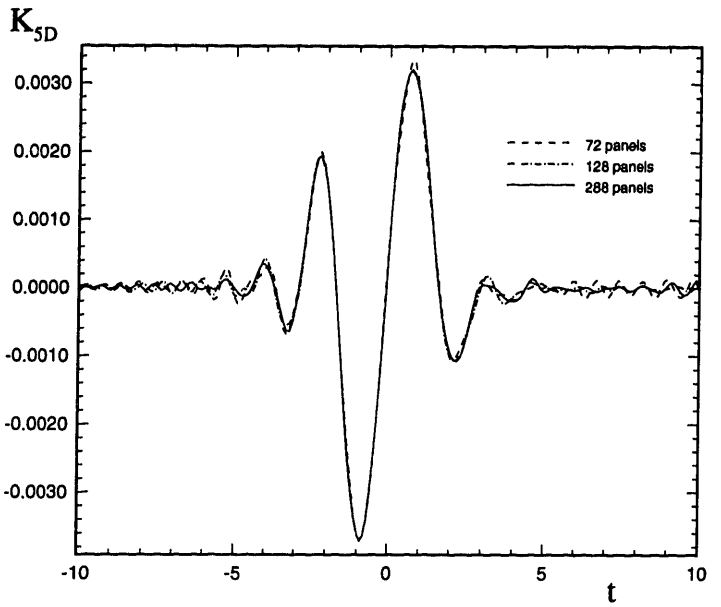

Figure 4-4: Pitch exciting moment impulse-response function for a Wigley hull travelling at $F_n = 0.0$ in head seas.

see the results are identical to graphical accuracy and so we may be fully confident with our numerical scheme for zero forward speed.

4.2 Forward Speed Results: Head Seas

Turning our attention to the more interesting case of a body in steady forward translation, we first look at this body in head seas. Time-domain results for the diffraction problem in head seas at forward speed have previously been shown by King [11]. There is also an existing pool of experimental and numerical data in the frequency domain. We will use this data to further verify our model.

Figures (4-7) and (4-8) illustrate convergence properties for typical heave and pitch diffraction impulse-response functions respectively. We see the results for three separate discretizations of a Wigley hull translating at a Froude number of 0.3. As is exemplified by these figures, it is possible to obtain practical results with a panelization of 144 panels over the half-body exploiting port/starboard symmetry. Temporal convergence occurs for a time step of 0.1.

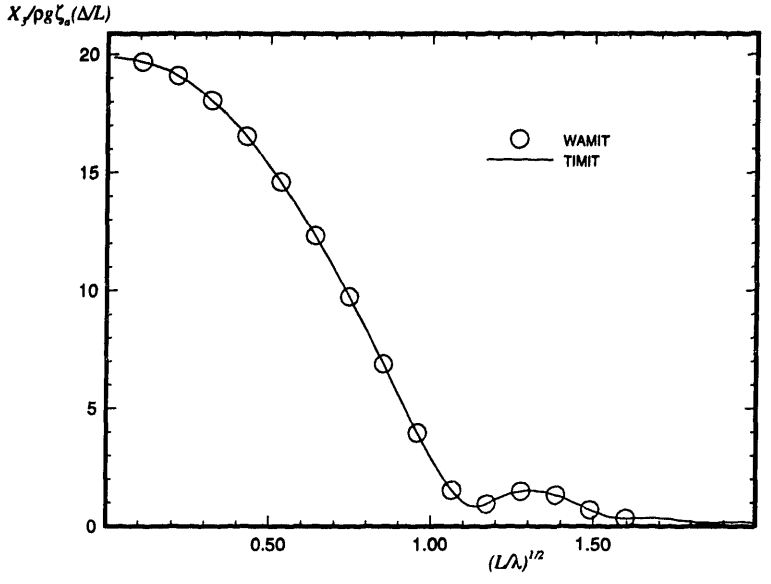

Figure 4-5: Heave exciting force amplitude for a Wigley hull travelling at $F_n = 0.0$ in head seas [2].

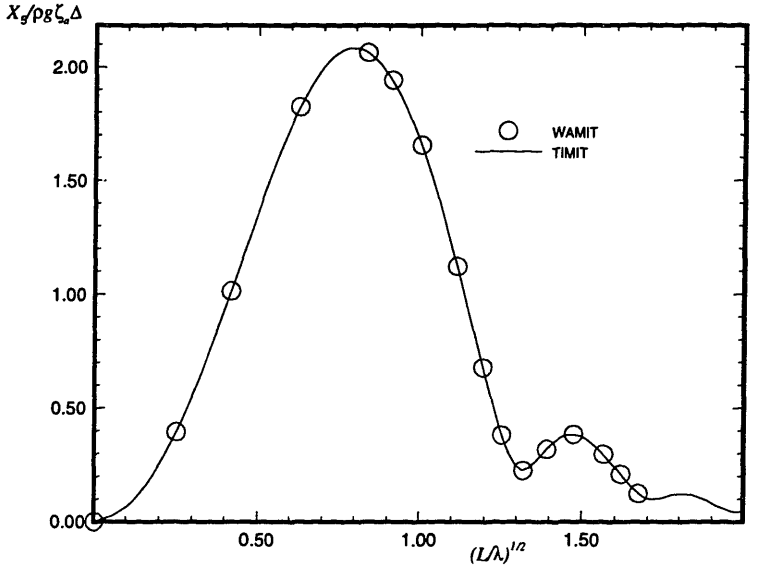

Figure 4-6: Pitch exciting moment amplitude for a Wigley hull travelling at $F_n = 0.0$ in head seas [2].

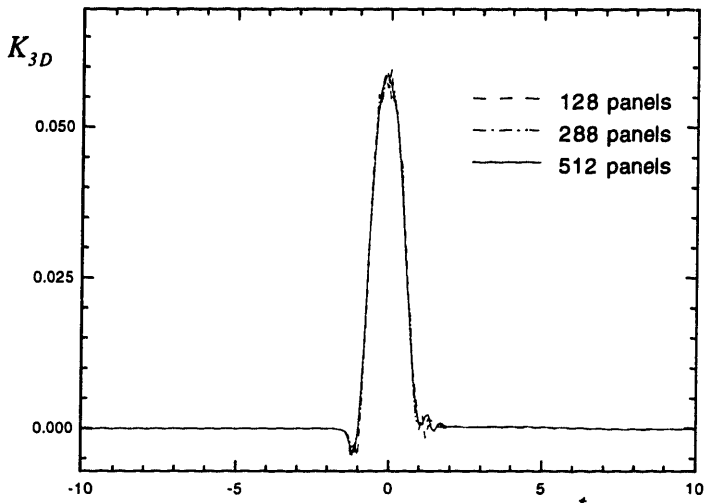

Figure 4-7: Convergence properties of the heave exciting force impulse-response function for a Wigley hull travelling at $F_n = 0.3$ in head seas [2].

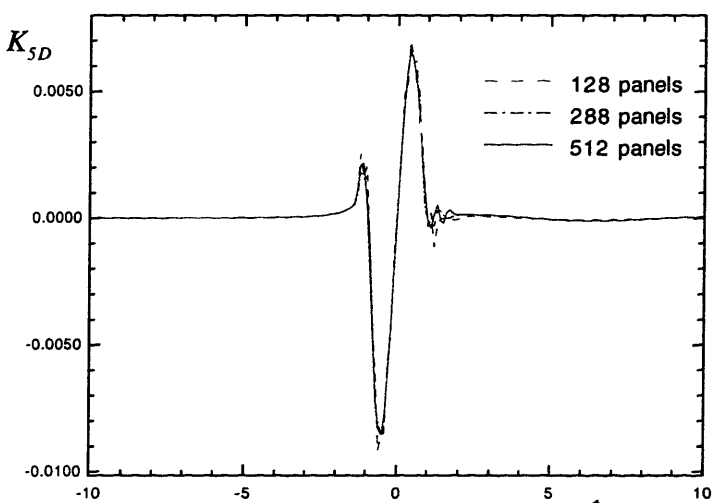

Figure 4-8: Convergence properties of the pitch exciting moment impulse-response function for a Wigley hull travelling at $F_n = 0.3$ in head seas [2].

A noteworthy aspect of the impulse-response functions shown in Figures (4-7) and (4-8) is the presence of non-zero oscillations for time $t < 0$. This characteristic, also seen in the zero speed results, is due to the nature of the prescribed incident wave field. We saw earlier in section 3.3 that the incident wave field we have chosen is an amalgamation of all possible wave frequencies and is defined such that all of these waves come together at the ship's origin at time $t = 0$. As a consequence, the bow of the ship passes into the wave field for $t < 0$ while there is still some dispersion. Hence, the bow experiences some excitation before $t = 0$ and these excitations show up as small pre-peak oscillations.

The effect discussed above may best be illustrated by Figures (4-9) and (4-10). Here we see both heave exciting force and pitch exciting moment impulse-response functions for different levels of forward speed, the fastest being at a Froude number of 0.4 and the slowest being zero speed. Note that as the ship moves at faster forward speeds, the peak becomes higher and sharper with the onset of pre-peak oscillations coming at a time closer to $t = 0$. This phenomenon is a manifestation of the ship moving in the opposite direction to the incident wave field and the fact that we have defined the incident potential with respect to the ship-fixed coordinate system. Because the oncoming wave field is timed to coalesce at $t = 0$ and the wave field is described by the encounter frequency, the bow of the faster moving ship arrives when the waves are less dispersed and hence feels less of the pre-peak effect. Likewise, the more complete or "tighter" coalescence results in the ship experiencing more energy closer to the peak.

We may obtain frequency-domain results from our impulse-response functions by making use of the Fourier transform:

$$X_j(\omega_e) = \int_{-\infty}^{\infty} dt K_{jD}(t) e^{-i\omega_e t} \tag{4.2}$$

where the exciting forces (or moments) are now a function of encounter frequency. These forces are most useful to us as a function of absolute frequency and may

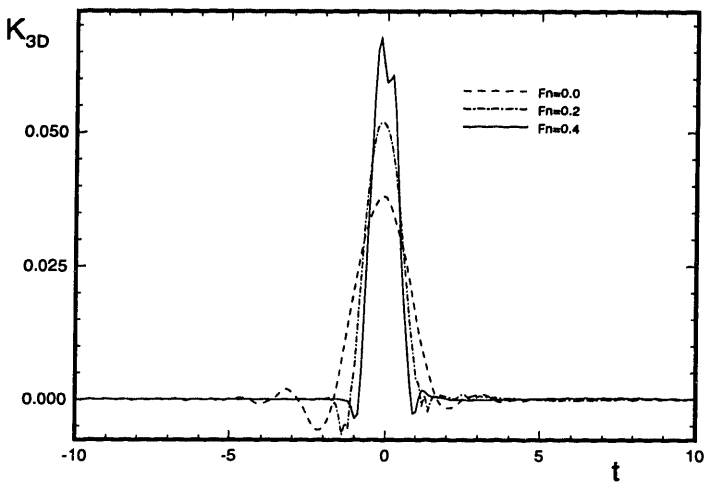

Figure 4-9: Comparison of heave exciting force impulse-response functions for a Wigley hull travelling at different forward speeds in head seas.

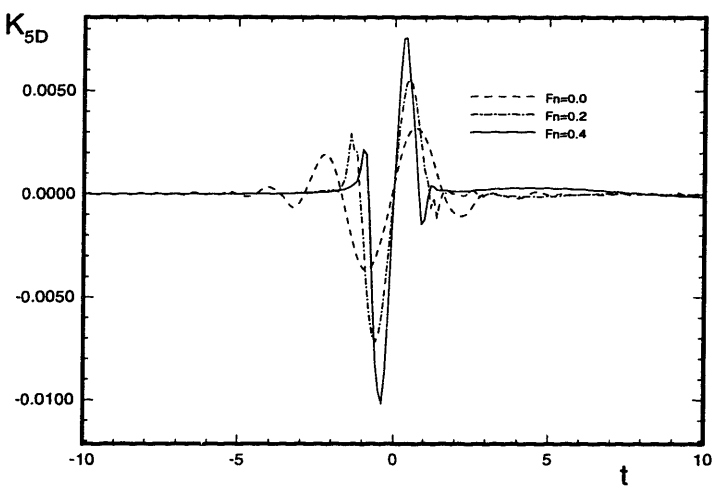

Figure 4-10: Comparison of pitch exciting moment impulse-response functions for a Wigley hull travelling at different forward speeds in head seas.

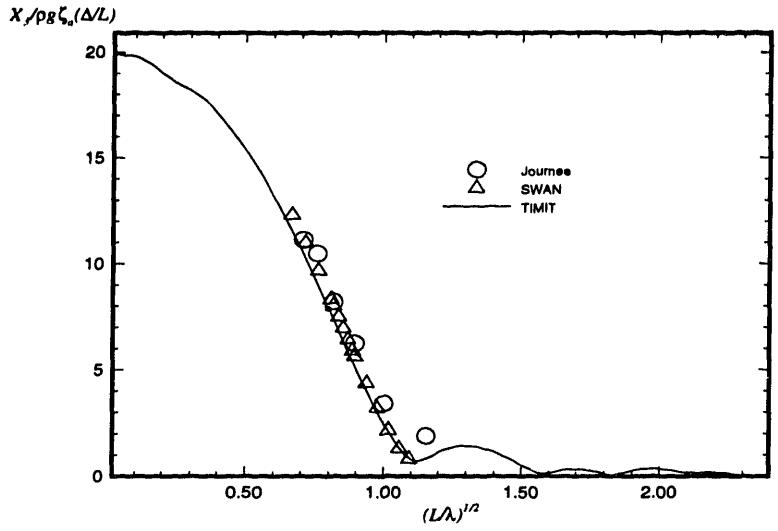

Figure 4-11: Heave exciting force amplitude for a Wigley hull travelling at $F_n = 0.3$ in head seas [2].

easily be converted as such given the relation in (2.84). Figures (4-11) and (4-12) show the magnitude of frequency-domain exciting force and pitch exciting moment for a Wigley hull at a Froude number of 0.3. Similar plots for phase angle may be found in Figures (4-13) and (4-14). In both sets of plots, T$\bar{\text{I}}$MIT results are compared with experimental data of Journée [10] and numerical results from the Rankine panel method SWAN [14]. Agreement in the case of heave exciting force, both magnitude and phase angle, is quite good. The results for pitch exciting moment amplitude are not as nice, however. The reason for the discrepencies may lie in the method of the calculation of the m-terms which affect the force computation as seen in equation (2.49). While T$\bar{\text{I}}$MIT uses a Neumann-Kelvin linearization, SWAN employs a linearization about the double-body flow. Because the value of the m-term vanishes for heave but is nonzero for pitch, the difference in linearization schemes may explain the better agreement with experiment for pitch demonstrated by SWAN [2].

The final set of results presented for head seas are those obtained from the simulation of a Wigley hull moving through a seaway at a Froude number of 0.3. The wave spectrum used is a Pierson-Moskowitz corresponding to a wind speed of 5 meters per second. A portion of the time history for the input wave elevation along with

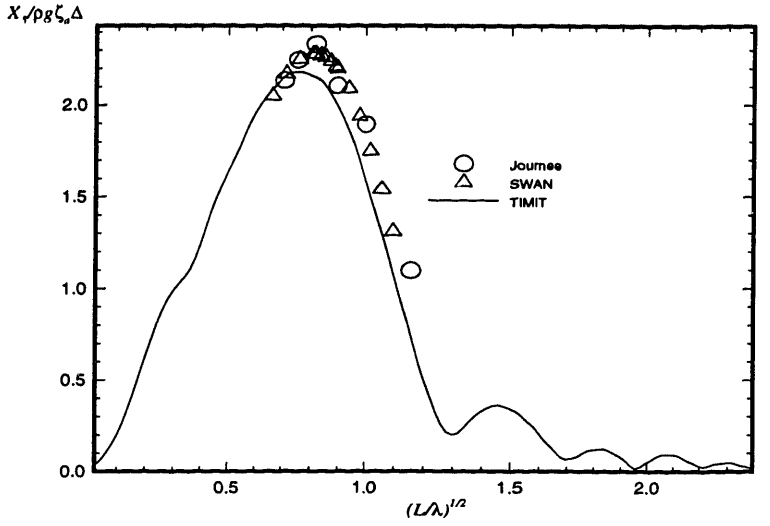

Figure 4-12: Pitch exciting moment amplitude for a Wigley hull travelling at $F_n = 0.3$ in head seas [2].

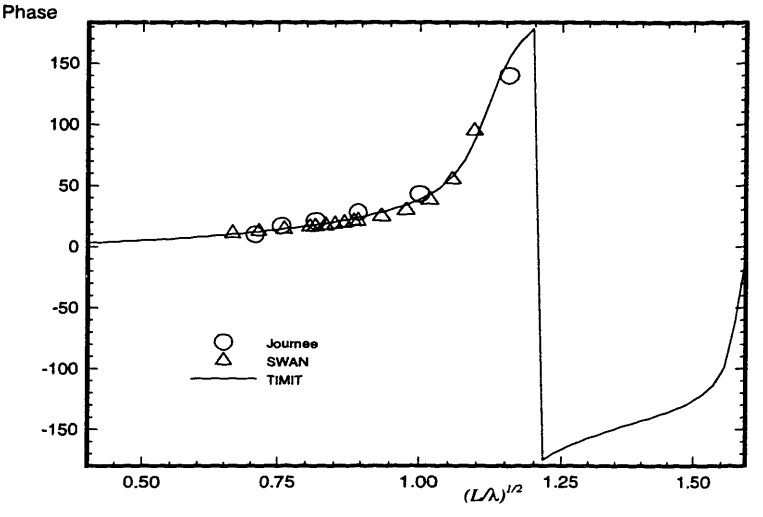

Figure 4-13: Heave exciting force phase angle for a Wigley hull travelling at $F_n = 0.3$ in head seas [2].

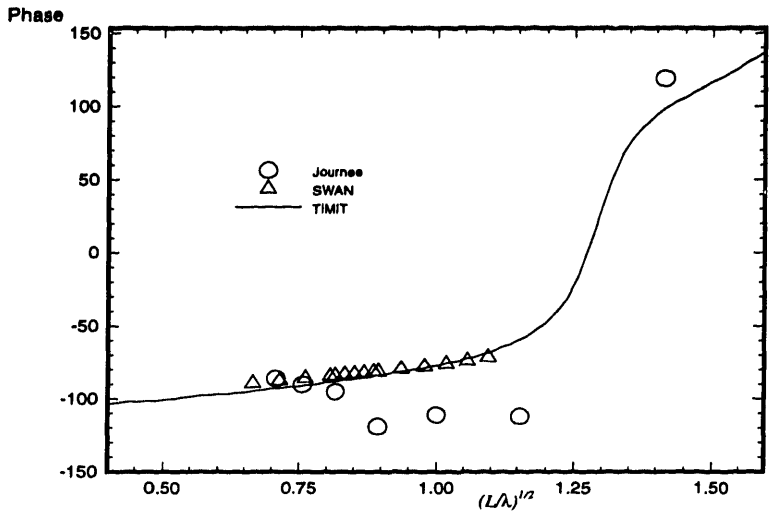

Figure 4-14: Pitch exciting moment phase angle for a Wigley hull travelling at $F_n = 0.3$ in head seas [2].

heave and pitch responses are shown in Figure (4-15). As previously mentioned, we can obtain frequency-domain response amplitude operators by using equation (3.66). Response amplitude operators corresponding to the input and output in figure (4-15) may be found in Figures (4-16) and (4-17). Plotted along with these results are experimental data from Journée [10]. One notable characteristic of these plots is the slow convergence around the resonant peak. This effect may be attributed to two numerical phenomena involving the solution of the discrete equations of motion - poor conditioning of the linear system in the region of resonant response and sensitivity in time step size for the numerical integration scheme [2].

4.3 Forward Speed Results: Following Seas

Finally, we look at the more complex situation of a body in steady forward translation encountering following seas. Experimental time-domain results for this case are not readily available. Likewise, frequency-domain experimental data are in short supply so verification of our numerical results is difficult and we must rely a great deal on intuition.

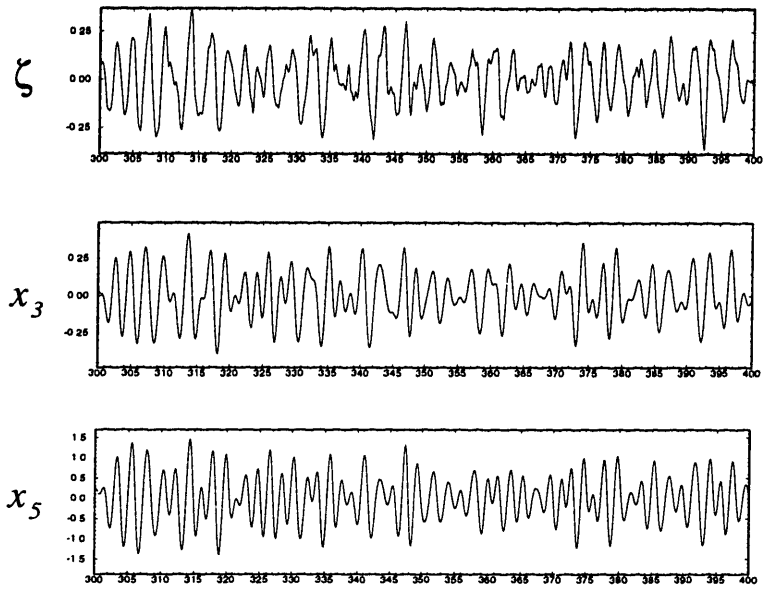

Figure 4-15: Sample data for the simulation of a Wigley hull travelling at $F_n = 0.3$ in head seas. The top plot is the input incident wave field in the ship-fixed frame, the middle plot is the heave response, and the bottom plot is the pitch response [2].

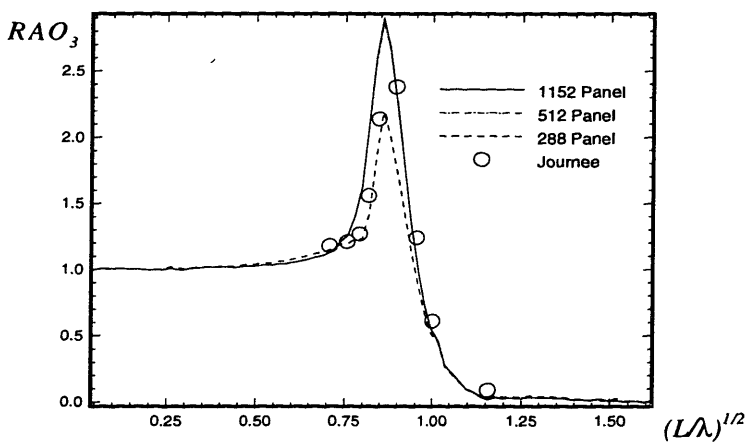

Figure 4-16: Response amplitude operator for the heave exciting forces of a Wigley hull travelling through a Pierson-Moskowitz wave spectrum at $F_n = 0.3$ and $\beta = \pi$ [2].

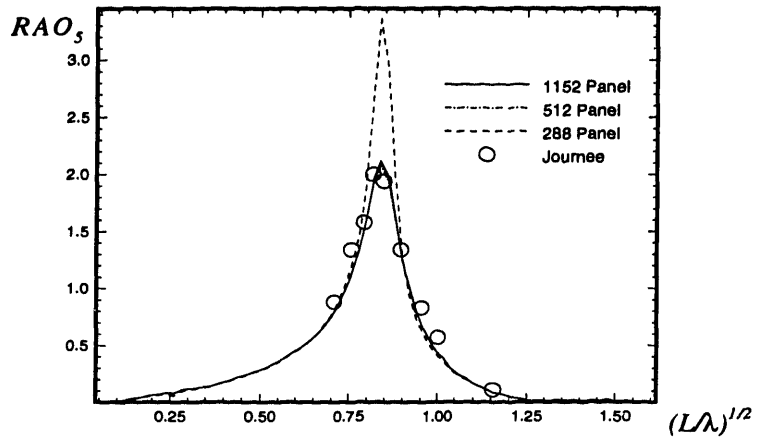

Figure 4-17: Response amplitude operator for the pitch exciting moments of a Wigley hull travelling through a Pierson-Moskowitz wave spectrum at $F_n = 0.3$ and $\beta = \pi$ [2].

Let us first examine the typical convergence behavior for the time-domain impulse-response functions. We recall that for following seas we need three separate impulse-response functions for each mode of motion to account for the ambiguity in absolute frequency. Figures (4-18), (4-19), and (4-20) show heave impulse-response functions for three discretizations of a Wigley hull translating at a Froude number of 0.3. Similar plots for pitch may be found in Figures (4-21), (4-22), and (4-23). The most interesting trend we see in these figures is the generally fast convergence for the impulse-response functions that relate to the two lower frequency ranges of incident wave input (Figures (4-18), (4-19), (4-21), and (4-22)) as contrasted to the poorer convergence found in the higher frequency range results (Figures (4-20) and (4-23)). The relatively slow convergence found in this range of high frequencies may be attributed to the high frequency wave effects discussed earlier. More specifically, as the body discretization becomes finer (and consequently the panels become smaller), the effects of the smaller wavelength high frequency waves are better represented in the numerical results.

In the previous section, we saw that for head seas the peak of the impulse-response

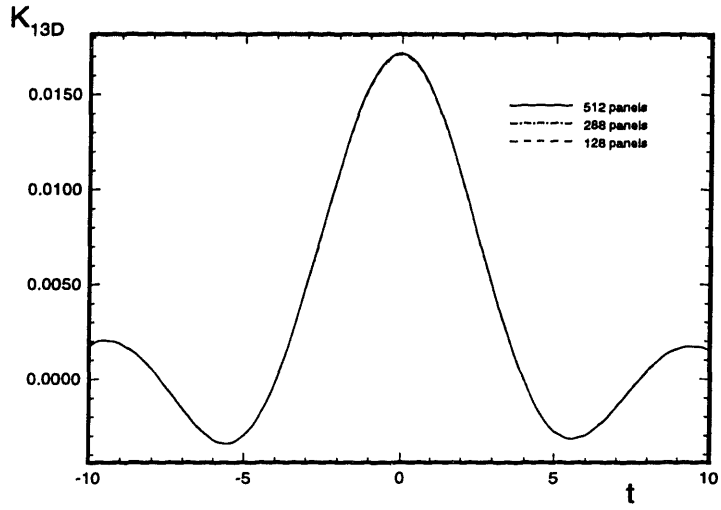

Figure 4-18: Convergence properties of the heave exciting force impulse-response function for a Wigley hull travelling at $F_n = 0.3$ in following seas where $0 \leq \omega_1 \leq \frac{g}{2U\cos\beta}$.

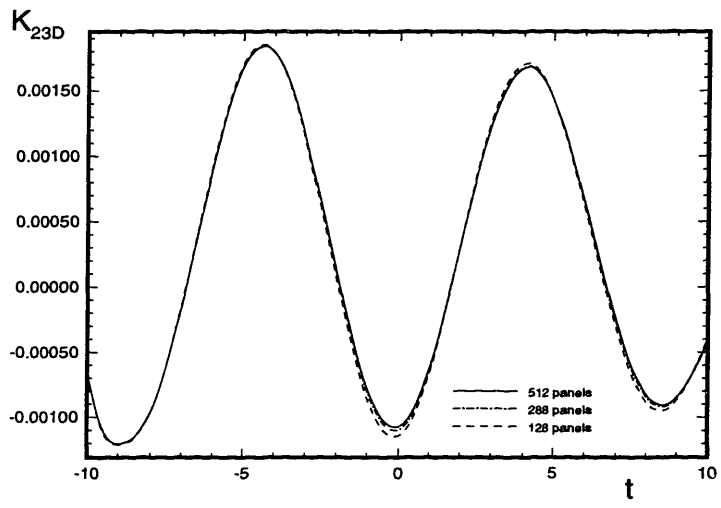

Figure 4-19: Convergence properties of the heave exciting force impulse-response function for a Wigley hull travelling at $F_n = 0.3$ in following seas where $\frac{g}{2U\cos\beta} \leq \omega_2 \leq \frac{g}{U\cos\beta}$.

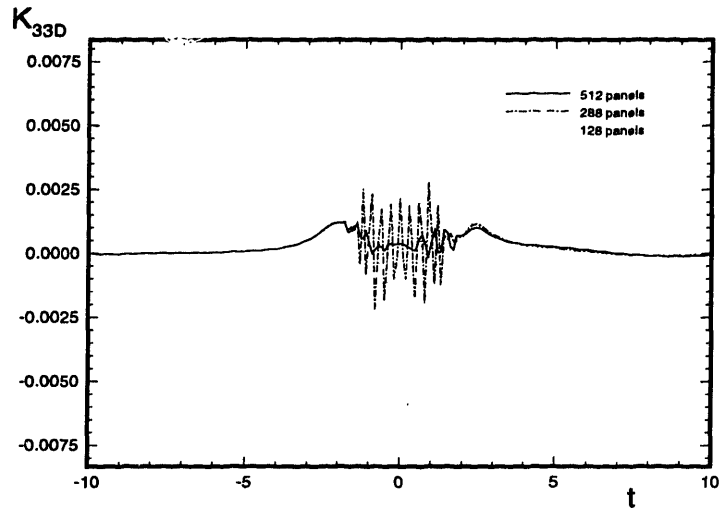

Figure 4-20: Convergence properties of the heave exciting force impulse-response function for a Wigley hull travelling at $F_n = 0.3$ in following seas where $\frac{g}{U\cos\beta} \leq \omega_3 \leq \infty$.

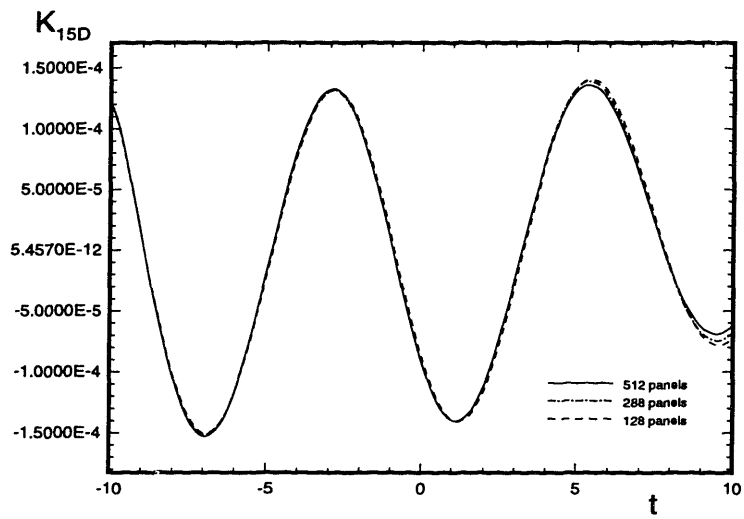

Figure 4-21: Convergence properties of the pitch exciting moment impulse-response function for a Wigley hull travelling at $F_n = 0.3$ in following seas where $0 \leq \omega_1 \leq \frac{g}{2U\cos\beta}$.

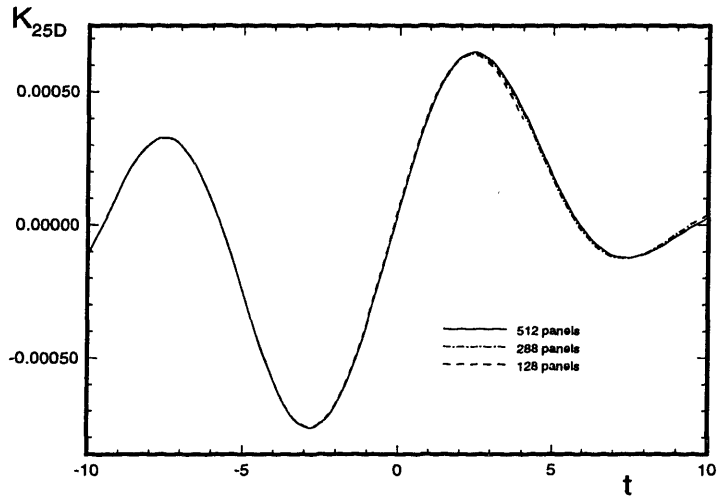

Figure 4-22: Convergence properties of the pitch exciting moment impulse-response function for a Wigley hull travelling at $F_n = 0.3$ in following seas where $\frac{g}{2U\cos\beta} \leq \omega_2 \leq \frac{g}{U\cos\beta}$.

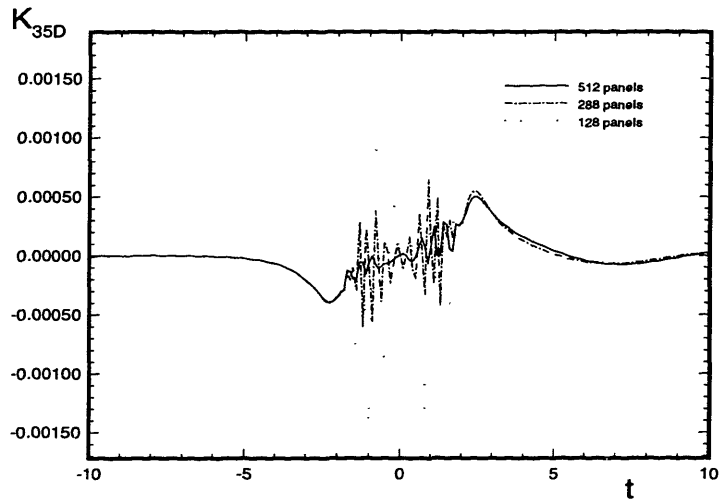

Figure 4-23: Convergence properties of the pitch exciting moment impulse-response function for a Wigley hull travelling at $F_n = 0.3$ in following seas where $\frac{g}{U\cos\beta} \leq \omega_3 \leq \infty$.

function became higher and narrower as the ship's speed increased. One might then expect to find an analogous trend as ship speed increases in following seas. This is indeed the case. We can see from Figures (4-24) and (4-25), which are comparisons of heave and pitch impulse-response functions for the input frequency range of $0 \leq \omega_1 \leq \frac{g}{2U\cos\beta}$, that as Froude number increases, the peak spreads out more and becomes lower. The explanation for this behavior is similar to that found for head seas, but here the situation is reversed. The ship is now travelling within an incident wave field containing one frequency range of waves with group speed greater than ship speed and two frequency ranges of waves with group speed less than ship speed(see section 2.7 for more detail). Given this condition, the faster the ship travels, the longer it will take for the overtaking wave groups to reach the vessel's origin and point of wave coalescence. Likewise, as the ship's speed increases, there will be fewer wave groups which fall into the overtaking category. Hence, the stern of the ship experiences more pre-peak response and for similar reasons the bow experiences more post-peak response. The end result is that the energy is more broadly spread around the zero time region.

Conversely, we see a seemingly opposite effect in the peak area for the two frequency ranges of wave groups which travel slower than the ship's speed, i.e., the wave frequencies described by ω_2 and ω_3. In this case, the ship is catching up with the wave groups in these frequency ranges and so the faster the ship travels, the quicker it should overtake them. There will be more wave groups to overtake, however. Thus we see greater peak responses in these ranges for faster ship speeds, but we also see some of the broadening found in the first range response. Figures (4-26) and (4-27), which are comparisons of heave and pitch impulse-response functions for the input frequency range of $\frac{g}{2U\cos\beta} \leq \omega_2 \leq \frac{g}{U\cos\beta}$, illustrates these points, although the response for this frequency range is dominated by $\tau = \frac{1}{4}$ effects.

As mentioned above, one of the most striking features of the figures previously presented is the magnitude of the oscillations occurring both behind and ahead of the peak. We may attribute these oscillations to the $\tau = \frac{1}{4}$ wave frequency. It should be noted that for head seas, the $\tau = \frac{1}{4}$ effects for the Wigley hull are minimal since

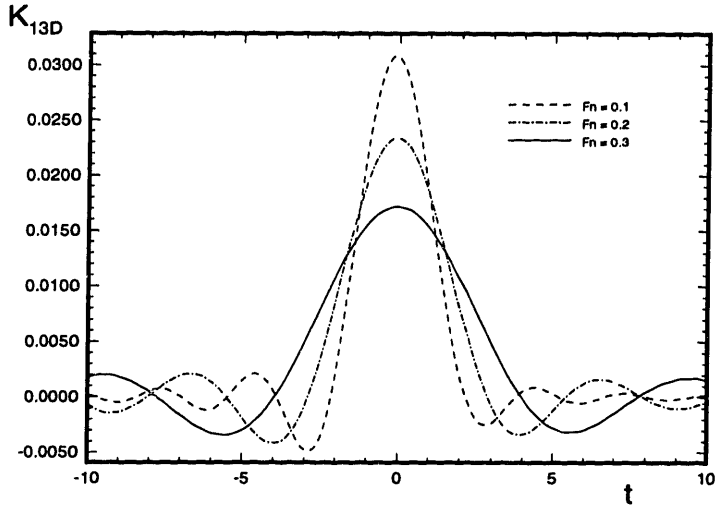

Figure 4-24: Comparison of heave exciting force impulse-response functions for a Wigley hull travelling at different forward speeds in following seas where $0 \leq \omega_1 \leq \frac{g}{2U\cos\beta}$.

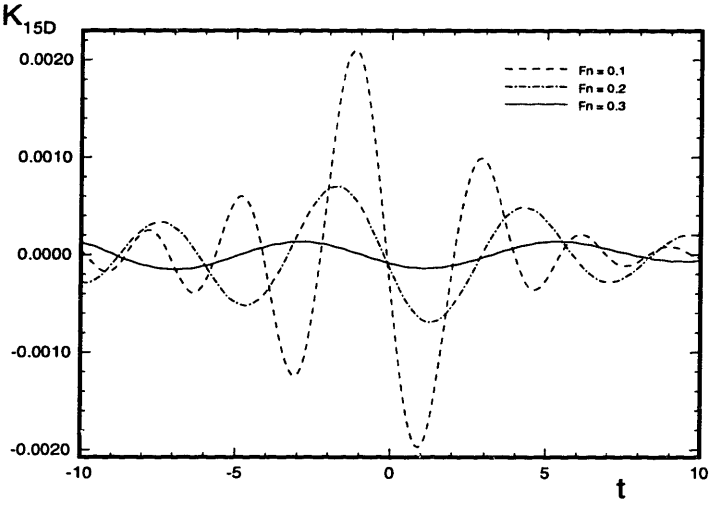

Figure 4-25: Comparison of pitch exciting moment impulse-response functions for a Wigley hull travelling at different forward speeds in following seas where $0 \leq \omega_1 \leq \frac{g}{2U\cos\beta}$.

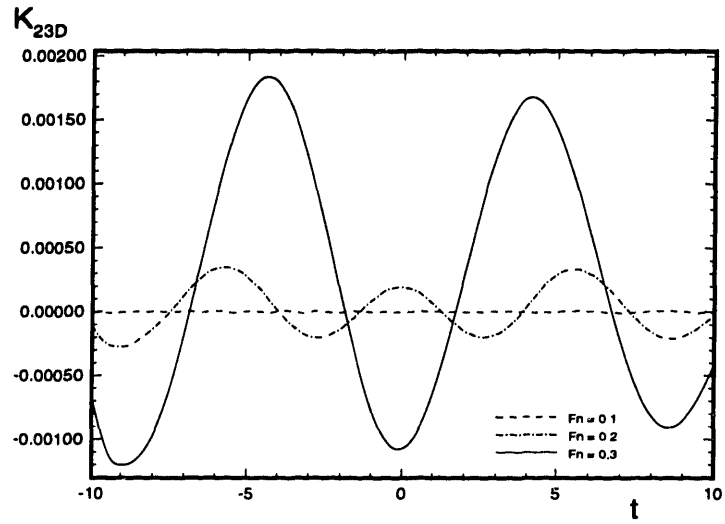

Figure 4-26: Comparison of heave exciting force impulse-response functions for a Wigley hull travelling at different forward speeds in following seas where $\frac{g}{2U\cos\beta} \leq \omega_2 \leq \frac{g}{U\cos\beta}$.

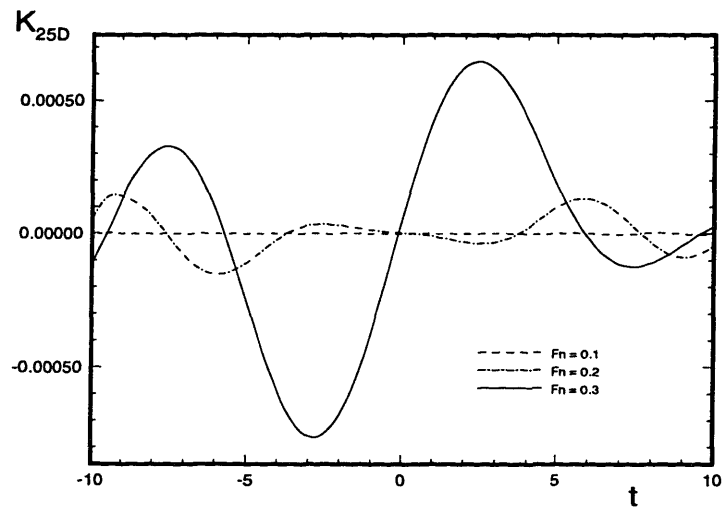

Figure 4-27: Comparison of pitch exciting moment impulse-response functions for a Wigley hull travelling at different forward speeds in following seas where $\frac{g}{2U\cos\beta} \leq \omega_2 \leq \frac{g}{U\cos\beta}$.

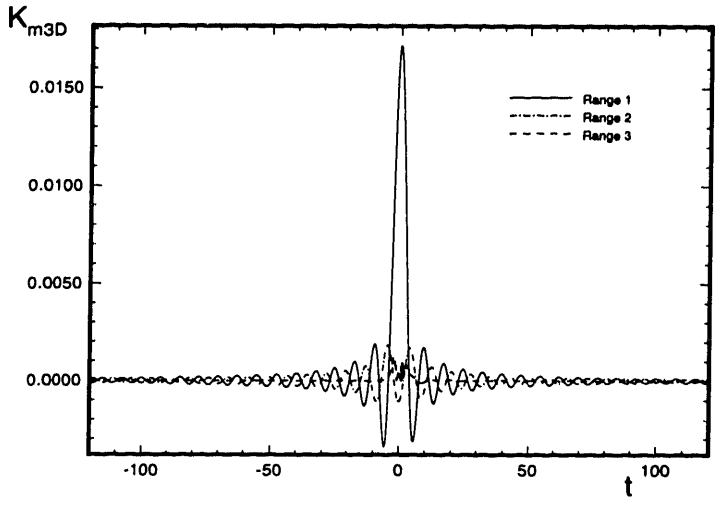

Figure 4-28: Extended time histories of the heave exciting force impulse-response functions for a Wigley hull travelling at $F_n = 0.3$ in following seas.

this hull form is a very weak scatterer, i.e., the scattering effects of the Wigley hull in head seas is an order of magnitude smaller than the Froude-Krylov forces created by the incident wave field. In following seas, however, the nature of the incident wave field and the definition of where and when it coalesces result in the ship always riding on the wave which has the same group speed as the ship's forward velocity. We recall from section 2.7 that this group speed corresponds to the frequency where the $\tau = \frac{1}{4}$ singularity occurs. Therefore, the ship always experiences a response associated with this wave group - a response which grows as the wave groups get closer together and shrinks as the wave groups disperse.

The short time duration shown in the earlier figures does not allow us to understand the complete behavior of the $\tau = \frac{1}{4}$ oscillations. Thus it is necessary to examine a substantially longer time history of the impulse-response function. Such time histories are presented in Figures (4-28) and (4-29) for heave and pitch respectively. Bingham et al. [2] shows that for forward speed, the leading order of the Green function is described asymptotically by the expression

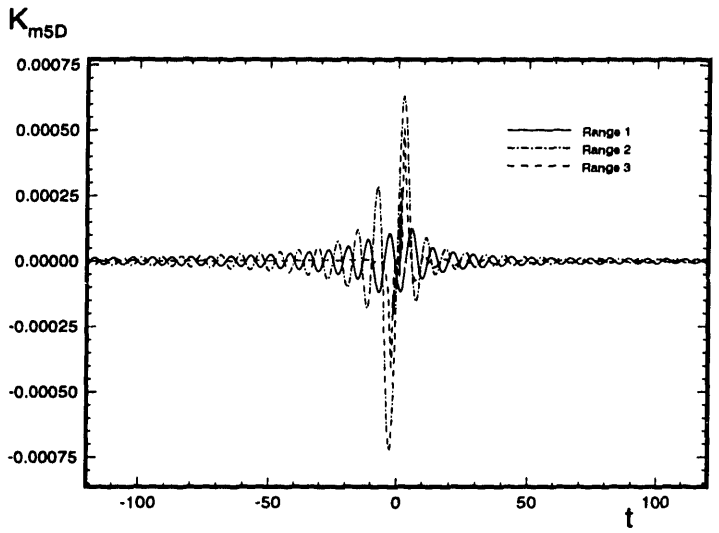

Figure 4-29: Extended time histories of the pitch exciting moment impulse-response functions for a Wigley hull travelling at $F_n = 0.3$ in following seas.

$$G_t \sim \frac{\sqrt{2}}{U^2 t} e^{\frac{g}{4U^2}} \sin(\omega_c t), \tag{4.3}$$

where $\omega_c = \frac{g}{4U}$ is the critical frequency of oscillation. This behavior leads to the postulation that the $\tau = \frac{1}{4}$ oscillations should also decay proportional to $\frac{1}{t}$. A cursory examination of the data presented in Figures (4-28) and (4-29) shows this to be true. One aspect of these oscillations which may not be intuitively obvious is that the contributions from the ω_1 frequency range and the ω_2 frequency range appear to be out of phase by 180 degrees. A closer look at the equations governing the forcing of this problem, i.e, the spatial and temporal derivatives of the incident potential, shows us why the oscillations behave as such. In particular, let us examine the expressions for $\vec{\nabla}\phi_1^I$ and $\vec{\nabla}\phi_2^I$ found in equations (3.7) and (3.8) respectively. We note that in the case of $\vec{\nabla}\phi_1^I$, the $\tau = \frac{1}{4}$ frequency contributes to the quantity as the upper limit of integration. In the case of $\vec{\nabla}\phi_2^I$, however, the $\tau = \frac{1}{4}$ frequency contributes to the quantity as the lower limit of integration. We should also remember that

at this frequency the integrands in the equations for $\vec{\nabla}\phi_1^I$ and $\vec{\nabla}\phi_2^I$ are the same. Thinking only in the mathematical terms of evaluating these integrals, it should then become apparent that the contribution of the $\tau = \frac{1}{4}$ frequency in equations (3.7) and (3.8), which begins to dominate at times far from $t = 0$, should be of opposite sign and similar magnitude. This reasoning is born out further by the analytical expressions for these quatities found in section 3.3, however, it should not imply that these expressions cancel each other.

As with the case of head seas, we may obtain results for following seas in the frequency domain by taking Fourier transforms of the individual impulse-response functions. These transforms are represented as

$$X_{mj}(\omega_e) = \int_{-\infty}^{\infty} dt K_{mjD}(t) \mathrm{e}^{-i\omega_e t}$$

$$\text{for} \quad m = 1, 2, 3, \tag{4.4}$$

where m corresponds to the three distinct input frequency ranges. Again, the exciting forces or moments are a function of encounter frequency. These frequency-domain results are shown for heave and pitch in Figures (4-30) and (4-31). Because input for the impulse-response functions corresponding to the first and second frequency ranges ($m = 1$ and 2) only has frequency content $0 \leq \omega_e \leq \frac{g}{4U\cos\beta}$, we expect to see no response beyond this region for these functions and this is indeed the case. Likewise, because input for the impulse-response function corresponding to the third frequency range ($m = 3$) contains all encounter frequencies, we are not surprised to see response across the entire spectrum.

It is possible to obtain frequency-domain results with respect to absolute frequency by using the relations found in eqations (2.96), (2.97), and (2.98). Such results are shown in Figures (4-32) and (4-33) for heave and Figures (4-34) and (4-35) for pitch.

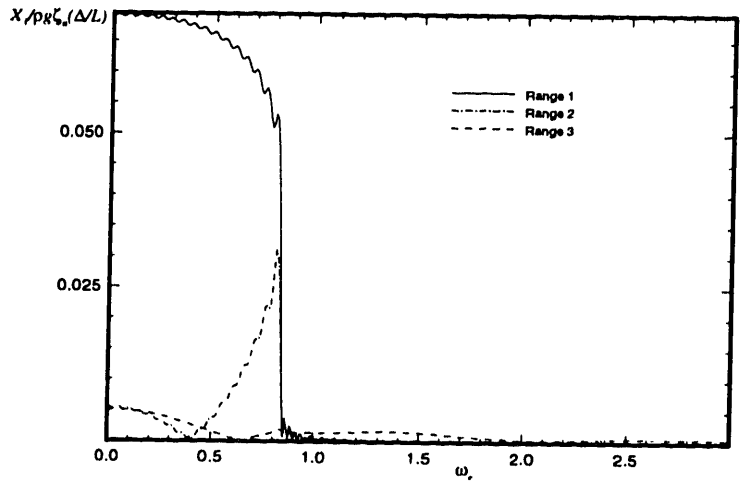

Figure 4-30: Heave exciting force amplitudes for a Wigley hull travelling at $F_n = 0.3$ in following seas.

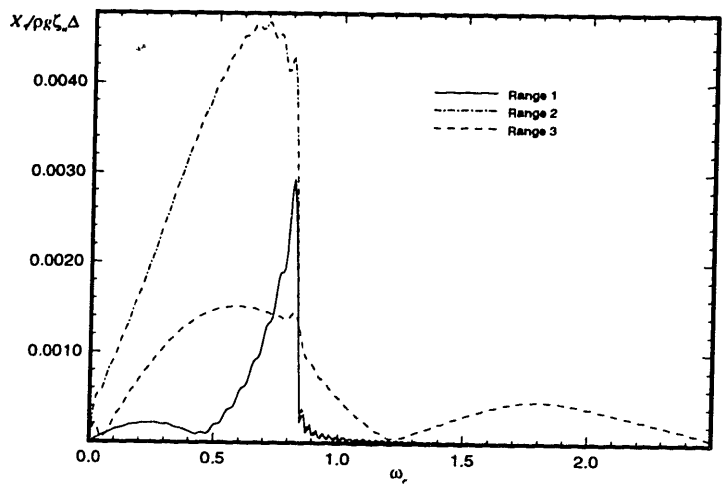

Figure 4-31: Pitch exciting moment amplitudes for a Wigley hull travelling at $F_n = 0.3$ in following seas.

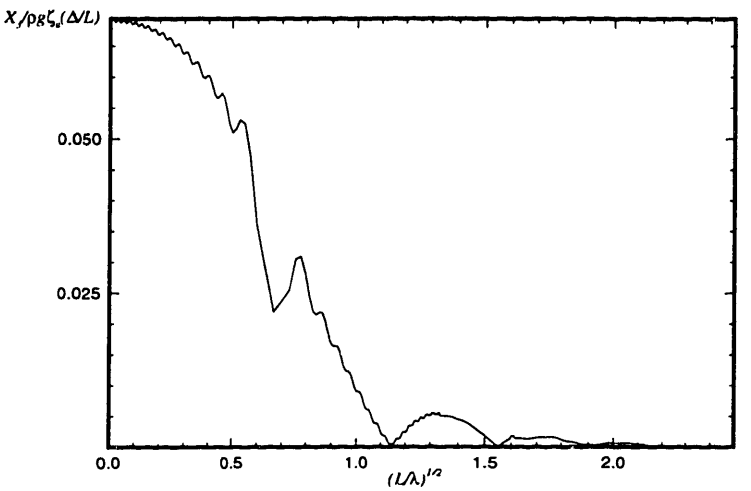

Figure 4-32: Heave exciting force amplitude with respect to absolute frequency for a Wigley hull travelling at $F_n = 0.3$ in following seas.

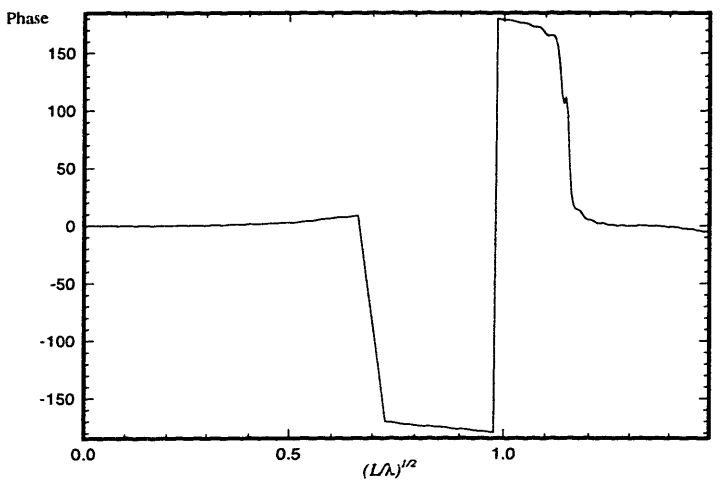

Figure 4-33: Heave exciting force phase angle with respect to absolute frequency for a Wigley hull travelling at $F_n = 0.3$ in following seas.

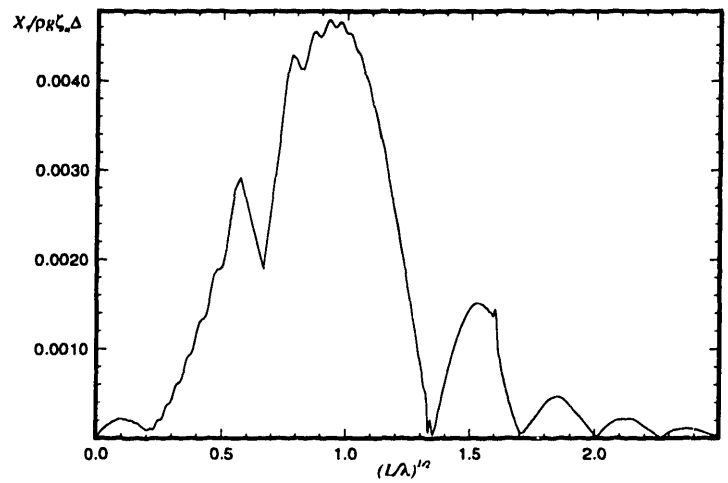

Figure 4-34: Pitch exciting moment amplitude with respect to absolute frequency for a Wigley hull travelling at $F_n = 0.3$ in following seas.

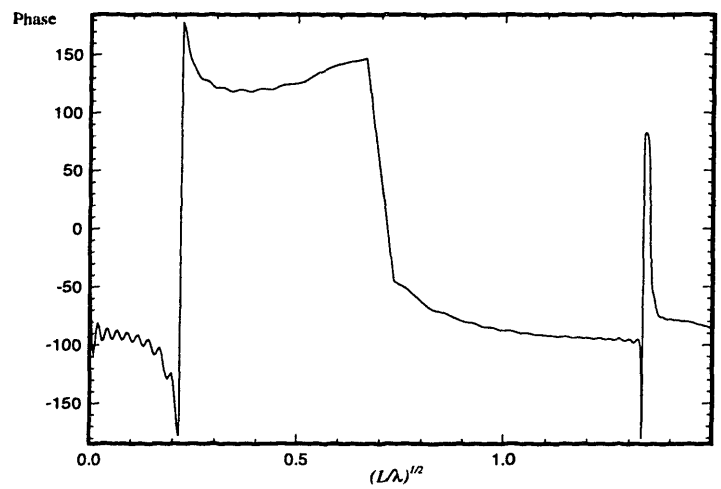

Figure 4-35: Pitch exciting moment phase angle with respect to absolute frequency for a Wigley hull travelling at $F_n = 0.3$ in following seas.

Chapter 5

Conclusions

In this thesis, we have achieved the objective of solving for the forces created by the diffraction problem in general, and in particular, have extended the problem for the special case of following seas. The approach used here is based on linear time-domain theory and solves for the velocity potential due to an incident wave field and its subsequent scattering by the body. The forces on the ship are then expressed in terms of impulse-response functions which allow us to determine the ship's reaction due to an arbitrary wave elevation. The theory is applicable to both the zero speed and forward speed cases.

Because we are using linearized potential flow theory, we must bear in mind that several simplifying assumptions have been made. By virtue of the potential flow, we have assumed that the fluid is incompressible and inviscid, and that the flow is irrotational. Likewise, by assuming that the problem is linear, we have neglected the higher order terms in all boundary conditions. As long as we consider only small perturbations about the body's mean position, these assumptions are valid and produce accurate results.

Much of the theory presented in this thesis is known from previous work in the field of ship motions. An interesting new piece of theory, however, is found in the presentation of the forward speed Haskind relations in the time domain. These relations are analogous to their frequency-domain counterparts and carry the same drawback of having to assume that the body is thin. While this characteristic reduces the

practical uses of these relations, they are still of scientific interest.

The need for modification of the general theory when solving the forward speed diffraction problem in following seas has also been discussed. We determined that given an impulsive incident wave field described by a potential with respect to the ship-fixed coordinate system, we must solve for three impulse-response functions which correspond to three distinct ranges of absolute wave frequency. This modification must be made because of the ambiguity in encounter frequency that arises when the ship is travelling in following waves.

The complexity of the overall problem dictates that we cannot solve for the potential analytically. It is therefore necessary to develop a robust numerical scheme for the purpose of calculating the potentials and impulse-response functions. To do so, we have relied on a three-dimensional panel method with constant source strengths. The second kind Fredholm integral equations have been discretized in space and time to produce a set of linear equations for the velocity potentials of the body panels at each time step. These potentials may then be used in the linearized Bernoulli equation and integrated over the body to determine the impulse-response functions.

Numerical results produced by this scheme show excellent agreement with experimental results when such results exist. In the case of following seas, for which experimental data is not readily available, the results follow intuition. In all cases it is possible to get analogous frequency-domain information from the impulse-response functions by taking their Fourier transforms. We may also use these impulse-response functions, along with impulse-response functions obtained from solution of the radiation problem, to predict the ship's motions in an arbitrary wave field via simulation.

An obvious next step in this project is to experimentally obtain data for a ship travelling at forward speed in following waves. Unfortunately, reliable experimental results for such a case are not easily found. Other areas that merit further consideration include choice of incident wave potential and nonlinearization of the problem. The former area has been discussed to some extent in [2]. The latter area may be addressed partially by using a 'body-nonlinear' approach, i.e., solving the problem using the exact body boundary conditions at each time step. Both areas may prove

to be excellent topics for future research.

Bibliography

[1] M. Abramowitz and I. A. Stegun. *Handbook of Mathematical Functions.* Dover Press, New York, 1964.

[2] H. B. Bingham, F. T. Korsmeyer, J. N. Newman, and G. E. Osborne. The simulation of ship motions. In 6^{th} *Intl. Conf. on Numerical Ship Hydro.*, 1993.

[3] W. E. Cummins. The impulse response function and ship motions. *Schiffstecknik*, 9:101–109, 1962.

[4] Department of Ocean Engineering, Massachusetts Institute of Technology, Cambridge. *WAMIT; A radiation-diffraction panel program for wave-body interactions*, 1988.

[5] Department of Ocean Engineering, Massachusetts Institute of Technology, Cambridge, MA. *TĪMIT* , 1993.

[6] W. Froude. On the rolling of ships. *Transactions of the Institute of Naval Architecture*, 2:180–229, 1861.

[7] W. Gautschi. The complex error function. *Collected Algorithms from CACM*, 1969.

[8] M. D. Haskind. The exciting forces and wetting of ships in waves. *Izvestia Akademii Nauk SSSR, Otdelenie Tekhnicheskikh Nauk*, (7):65–79, 1957.

[9] J. L. Hess and A. M. O. Smith. Calculation of nonlifting potential flow about arbitrary three-dimensional bodies. *Journal of Ship Research*, 8(2):22–44, 1964.

[10] J. M. J. Journée. Experiments and calculations on four Wigley hullforms. Technical Report 909, Delft University of Technology, Ship Hydromechanics Laboratory, Delft, The Netherlands, 1992.

[11] B. W. King. Time-domain analysis of wave exciting forces on ships and bodies. Technical Report 306, The Department of Naval Architecture and Marine Engineering, The University of Michigan, Ann Arbor, Michigan, 1987.

[12] F. T. Korsmeyer, J. N. Newman, and G. E. Osborne. The linear, transient, free-surface wave diffraction problem. In preparation, 1994.

[13] A. Kriloff. A new theory of the pitching motion of waves, and of the stresses produced by this motion. *Transactions of the Institute of Naval Architecture*, 37:326–368, 1896.

[14] D. E. Nakos and P. D. Sclavounos. Ship motions by a three dimensional Rankine panel method. In *Eighteenth Symp. on Nav. Hydro.*, Ann Arbor, Michigan, 1990.

[15] J. N. Newman. The exciting forces on fixed bodies in waves. *Journal of Ship Research*, 6(4):10–17, 1962.

[16] J. N. Newman. The exciting forces on a moving body in waves. *Journal of Ship Research*, 9(3):190–199, 1965.

[17] T. F. Ogilvie. Recent progress toward the understanding and prediction of ship motions. In *The Fifth Symposium on Naval Hydrodynamics*, pages 3–128, Bergen, 1964.

[18] T. F. Ogilvie and E. O. Tuck. A rational strip theory for ship motions, part 1. Technical Report 013, The Department of Naval Architecture and Marine Engineering, The University of Michigan, Ann Arbor, Michigan, 1969.

[19] J. J. Stoker. *Water Waves.* Interscience Publishers, Inc., New York, 1957.

[20] V Volterra. Sur la theorie des ondes liquides et la methode de Green. *J. Math. Pures Appl.*, 13:1–18, 1934.

[21] J. V. Wehausen. Initial value problem for the motion in an undulating sea of a body with fixed equilibrium position. *Journal of Engineering Mathematics*, 1:1–19, 1967.

[22] J. V. Wehausen. The motion of floating bodies. *Ann. Rev. Fluid Mech.*, 3:237–268, 1971.

[23] J. V. Wehausen and E. V. Laitone. Surface waves. In *Handbuch der Physik*, pages 446–778. Springer, 1960.